

Special Section:

Ophiolites and Oceanic Lithosphere, with a focus on the Samail ophiolite in Oman

Key Points:

- N. Apennine ophiolite records the evolution from serpentinite to ophicalcite during continuous uplift and exposure on the seafloor
- Continental basement-derived fluids imprinted a chemical signature on serpentinites during initial stages of rifting and mantle upwelling
- Late stage mafic-derived fluids induced pronounced Si-metasomatism in ophicalcites

Supporting Information:

Supporting Information may be found in the online version of this article.

Correspondence to:

E. M. Schwarzenbach and G. L. Früh-Green,
esther.schwarzenbach@fu-berlin.de;
frueh-green@erdw.ethz.ch

Citation:

Schwarzenbach, E. M., Vogel, M., Früh-Green, G. L., & Boschi, C. (2021). Serpentinization, carbonation and metasomatism of ultramafic sequences in the Northern Apennine ophiolite (NW Italy). *Journal of Geophysical Research: Solid Earth*, 126, e2020JB020619. <https://doi.org/10.1029/2020JB020619>


Received 24 JUL 2020

Accepted 21 APR 2021

© 2021. The Authors.

This is an open access article under the terms of the [Creative Commons Attribution](#) License, which permits use, distribution and reproduction in any medium, provided the original work is properly cited.

Serpentinization, Carbonation, and Metasomatism of Ultramafic Sequences in the Northern Apennine Ophiolite (NW Italy)

Esther M. Schwarzenbach^{1,2} , Monica Vogel², Gretchen L. Früh-Green², and Chiara Boschi³

¹Institute of Geological Sciences, Freie Universität Berlin, Berlin, Germany, ²Department of Earth Sciences, ETH Zürich, Zürich, Switzerland, ³Institute of Geosciences and Earth Resources - CNR Pisa, Pisa, Italy

Abstract Fluid-rock interaction in ultramafic rocks considerably affects the chemical and isotopic composition of the oceanic lithosphere. We present a geochemical and petrological study of serpentinites and ophicalcites of the Northern Apennine ophiolite, Italy. This ophiolite sequence represents fragments of Jurassic oceanic lithosphere that have been denuded by low angle detachment faults, exposing peridotites on the ocean floor and triggering hydrothermal alteration. Seawater circulation is documented by (Jurassic) seawater-like $^{87}\text{Sr}/^{86}\text{Sr}$ values and $\delta^{13}\text{C}$ values of 1.1–3.0‰ in carbonate veins of the ophicalcites. Bulk rock ophicalcites have low $^{87}\text{Sr}/^{86}\text{Sr}$ values of 0.70489–0.70599, elevated SiO_2 contents, and talc druses filling calcite veins that record Si-metasomatism. In contrast, underlying serpentinites have $^{87}\text{Sr}/^{86}\text{Sr}$ values above Jurassic seawater values. Bulk rock δD and $\delta^{18}\text{O}$ values of ophicalcites and serpentinites suggest interaction with an evolved seawater-derived and/or magmatic fluid. These chemical signatures result from a complex history of serpentinization, carbonation, and metasomatism. Multiphase water-rock interaction includes infiltration of basement-derived fluids during initial mantle upwelling within an opening ocean basin, followed by localized high-temperature fluid infiltration, extensive seawater circulation resulting in carbonation, and oxidation near the seawater-exposed surface, and finally, fluid-rock interaction with overlying mafic lithologies leading to Si-metasomatism.

The studied sequence represents an excellent example of the evolution from serpentinite to ophicalcite during continuous uplift and exposure of ultramafic rocks on the seafloor and documents the complex hydrothermal evolution of ultramafic rocks associated with this process. The extensive chemical transformation of mantle peridotites likely has an impact on geochemical cycles and subduction zone processes.

1. Introduction

Ocean ridge spreading centers produce around 18 km³ of oceanic crust each year (Cogné & Humler, 2006). Although the majority of newly formed oceanic crust is composed of mafic lithologies, approximately 9%–20% of the crust formed along slow spreading ridges comprises serpentinized peridotite (Alt, Schwarzenbach, et al., 2013; Cannat et al., 1995, 2010). In these tectonic settings mantle rocks are exposed to seawater and altered via a complex interplay of magmatism, asymmetric extension, and detachment faulting, which is commonly linked to the formation of oceanic core complexes (Cannat, Sauter, et al., 2006; Früh-Green et al., 2018; John & Cheadle, 2010; Tucholke et al., 2008). During continuous mantle uplift, the ultramafic rocks undergo extensive chemical exchange with circulating fluids, resulting in pronounced chemical and mineralogical transformation (Früh-Green et al., 1990, 1996; Paulick et al., 2006; Schwarzenbach, Früh-Green, Bernasconi, Alt, & Plas, 2013). Seawater-rock interaction has been shown to influence the chemical evolution of the oceans (e.g., Früh-Green et al., 2004; von Damm, 1995) and circulation of seawater through mantle sequences affects rheology, strength, and seismic properties of the oceanic lithosphere (e.g., Escartin et al., 1997; Miller & Christensen, 1997). In addition, subduction of the altered oceanic lithosphere transports various elements into Earth's interior (e.g., Alt, Schwarzenbach, et al., 2013; Scambelluri et al., 2004), affecting arc magmatism (e.g., Ulmer & Trommsdorff, 1995) and the chemical and isotopic evolution of Earth's interior (e.g., Li et al., 2020).

Hydrothermal alteration in ultramafic rocks is primarily expressed by serpentinization—the reaction of the primary mantle minerals olivine and pyroxene with water to form a rock dominated by serpentine and

magnetite (Bach et al., 2004; Moody, 1976; O'Hanley, 1996). These reactions generally produce low-temperature, alkaline (pH ~9–11), Ca-, and H₂-rich fluids that induce carbonate formation upon interaction with seawater, such as those described from the Lost City hydrothermal field (LCHF) on the Atlantis Massif (AM) (Mid-Atlantic Ridge (MAR), 30°N; Kelley, Karson, et al., 2001; Ludwig et al., 2006). The LCHF represents one of the best examples of a modern serpentinite-hosted marine hydrothermal system and is characterized by up to 60 m high carbonate-brucite chimneys and towers that vent up to 95°C, high pH fluids and host diverse microbial communities (e.g., Brazelton et al., 2006; Kelley, Karson, Früh-Green, et al., 2005). Recent studies have shown that the evolution of peridotite-hosted hydrothermal systems is complex, commonly involving melt-rock interaction and a complex alteration history of serpentinization, talc metasomatism, carbonation, and low-temperature seafloor weathering and oxidation (e.g., Früh-Green et al., 2018; Paulick et al., 2006). In many cases, interaction of water with interspersed gabbroic intrusions causes wide-spread or localized high-temperature imprint and changes the chemical signatures of the basement rocks, as documented by distinct enrichments in Si, Al, Ca, and assemblages of Ca-rich amphibole, talc, and chlorite (Boschi et al., 2006a, 2006b; Rouméjon et al., 2018). In addition, high-temperature fluid-rock interaction associated with magmatism can produce extensive sulfide deposits (e.g., Garuti et al., 2008; Marques et al., 2007), whereas low-temperature serpentinization may facilitate formation of considerable amounts of microbially produced sulfide (e.g., Alt, Schwarzenbach, et al., 2013).

Here, we present a study of alteration processes and carbonate deposition in the Northern Apennine ophiolite in Italy with the aim to unravel its chemical evolution from serpentinite to opihalcite formation. Ophiolites are fragments of oceanic lithosphere that have tectonically been emplaced on the continent (Coleman, 1977). Due to their exceptional exposure, they can provide unique insight into magmatic and hydrothermal processes that took place on the seafloor. The Northern Apennine ophiolite is considered a relict of oceanic lithosphere formed in the Piemont-Ligurian ocean. Previous research showed that this sequence records an oceanic alteration history similar to that described in a number of ultramafic core complexes along the MAR (e.g., Alt, Crispini, et al., 2018; Karson et al., 2006; Schwarzenbach, Früh-Green, Bernasconi, Alt, & Plas, 2013). The ophiolite only experienced a weak Alpine metamorphic overprint that did not exceed prehnite-pumpellyite facies conditions and did not modify the marine signatures (e.g., Cortesogno, Gianelli, & Piccardo, 1975; Garuti et al., 2008; Strating, 1991). Our study builds on previous work (Schwarzenbach et al., 2012, 2013, 2018), which was based on carbon and sulfur geochemistry and provided initial evidence for extensive seawater infiltration and variations in temperatures and fluid regime that also facilitated microbial activity in the serpentinites. Here, we present strontium, oxygen, and hydrogen isotope bulk rock data and in situ major and trace element compositions, which provide new, comprehensive insights into the hydrothermal and temporal evolution of this ophiolite sequence and the origin of the fluids that caused rock alteration. In particular, the good exposure of this sequence allows us to track its hydrothermal evolution during continuous uplift and exposure on the Jurassic ocean floor and the transition from serpentinite to opihalcite formation. We compare this ancient system with the AM, which provides a modern analog for the N. Apennine ophiolite and allows us to evaluate the interplay of serpentinization, metasomatism, and carbonation, and their effects on mass transfer during the hydrothermal evolution of ultramafic rocks. This allows us to better understand the chemical evolution of the oceanic lithosphere, which is eventually subducted along convergent margins and effectively controls long-term geochemical cycles.

2. Geological Overview and Samples

2.1. Regional Geology

The ophiolite successions in the N. Apennine (Eastern Liguria, Italy) represent relicts of a former oceanic lithosphere of the Ligurian Tethys that separated the European and Apulian continental plates during the Late Jurassic-Cretaceous and locally developed a slow- to ultraslow-spreading ridge (Lagabriele & Lemoine, 1997; Strating, 1991; Tribuzio, Thirlwall, & Vannucci, 2004). Along these spreading centers mantle exhumation was prevalent, whereas mature oceanic spreading was comparatively short-lived (Le Breton et al., 2021). Accordingly, these ophiolite sequences are characterized by a heterogeneous basement made up of gabbroic intrusions in mantle peridotites and are discontinuously overlain by opihalcites, basaltic lavas, sedimentary breccias, and pelagic sediments (e.g., B. E. Treves and Harper, 1994). The peridotite basement varies in composition from depleted spinel harzburgites to fertile spinel lherzolites, and from dunites

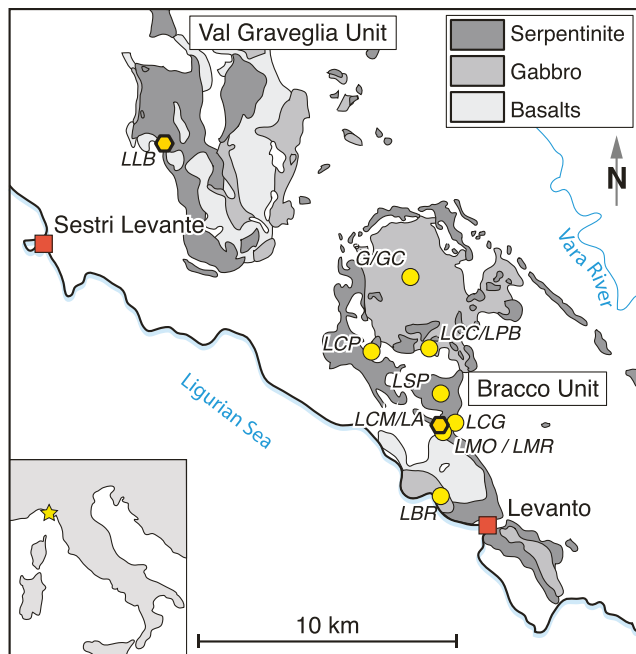


Figure 1. Geological map of the ophiolites in the Internal Liguride Units (N. Apennine, Italy) showing the Val Graveglia Unit to the northwest and the Bracco Unit to the southeast (modified from Garuti et al., 2008). Yellow circles and polygons: sampling sites and quarries. Yellow polygons mark Cava dei Marmi (LCM/LA) and the mining site near Libiola (LLB), where fault schists were sampled. Abbreviations: LBR–Bonassola; LCG–Cava Galli; LCP–Cava Piazza; LMO, LMR–Cava Montaretto; LSA–Cava S. Agata; LSP–Profile on road SS332; LPB, G, GC–Bracco Pass; LCC–Castagnola.

to plagioclase-enriched peridotites (Piccardo et al., 2014). MORB-type lavas form a thin and laterally discontinuous volcanic succession that was locally deposited directly on top of the mantle basement or the gabbros (Zaccarini & Garuti, 2008). Timing of gabbroic intrusions within the external and internal Ligurian units has been dated at 165–161 Ma based on U-Pb zircon ages and records the transition from an ocean-continent transition (OCT) zone to a slow-spreading ridge setting (Tribuzio, Garzetti, et al., 2016).

In the N. Apennine, the Internal Ligurian ophiolite units represent the oceanward fragments of oceanic lithosphere and include the Bracco and Val Graveglia Units (Figure 1). The Bracco Unit includes gabbroic intrusions in serpentinites that are discontinuously overlain by basaltic flows and pillow lavas with MORB affinity and Upper Jurassic to Cretaceous sediments (Cortesogno, 1981). The upper layer of the serpentinite basement becomes progressively more fractured, oxidized, and carbonated upwards, forming opihalcites. The opihalcite, also known as the Levanto Breccia, hosts an entangled polyphase complex of veins and fractures filled with calcite, talc, and a micritic to microsparitic matrix (Cortesogno, Galbiati, & Principi, 1980; B. E. Treves and Harper, 1994). Calcite precipitation occurred close to the seafloor surface where upwelling low-temperature hydrothermal fluids formed upon seawater-peridotite interaction and discharged through the fractured serpentinite basement (Schwarzenbach, Früh-Green, Bernasconi, Alt, & Plas, 2013). The opihalcites have been interpreted as extensional fault rocks and products of marine hydrothermal activity related to detachment faulting, which display evidence for an evolution from ductile to brittle deformation during cooling and decompression of the oceanic lithosphere (B. Treves et al., 1995; B. E. Treves and Harper, 1994). The Levanto Breccia is overlain by an upper sedimentary sequence, the Framura Breccia, which has sedimentary features, sedimentary dykes and infills, and is characterized by reworking of the underlying opihalcites.

The Val Graveglia Unit is situated northwest of the Bracco Massif and is characterized by serpentinitized peridotites, gabbros, pillow basalts, pillow breccias, and an Upper Jurassic to Cretaceous sedimentary cover. Additionally, the Val Graveglia Unit hosts massive sulfide deposits that include stratiform deposits, which overlie serpentinites or are associated with pillow basalts overlying the serpentinite and stockwork veins in gabbro and basalt (Garuti et al., 2008).

2.2. Sample Selection

Serpentinites, opihalcites, and fault rocks from the Bracco Unit were systematically sampled in several active or abandoned quarries (Figure 1) allowing for the recovery of fresh sample material unaffected by long-term weathering. Talc-tremolite fault schists were sampled from a dome-shaped structure in the Cava dei Marmi that represents a several meters-wide zone of strongly sheared fault rocks along the contact between the opihalcite and the overlying volcano-sedimentary sequence (from here on referred to as Cava dei Marmi fault schists). We classify the opihalcites into two groups according to their oxidation state and tectonic history: green and red opihalcites. The green opihalcites are defined here as completely serpentinitized and variably calcite-veined massive peridotites. They have been fractured in situ and are characterized by the presence of cross-cutting generations of calcite veins. Locally, oxidation is observed along the calcite veins (Figure 2a). The red opihalcites typically overlie the green opihalcites and are highly fractured, partly brecciated, and are interpreted as tectonic breccias (Figure 2b). They are characterized by an intense red color, crosscut by a myriad of calcite veins commonly containing talc in druses. The transition from serpentinites, to green and then to red opihalcites is gradual and reflected by an increase in calcite veining and

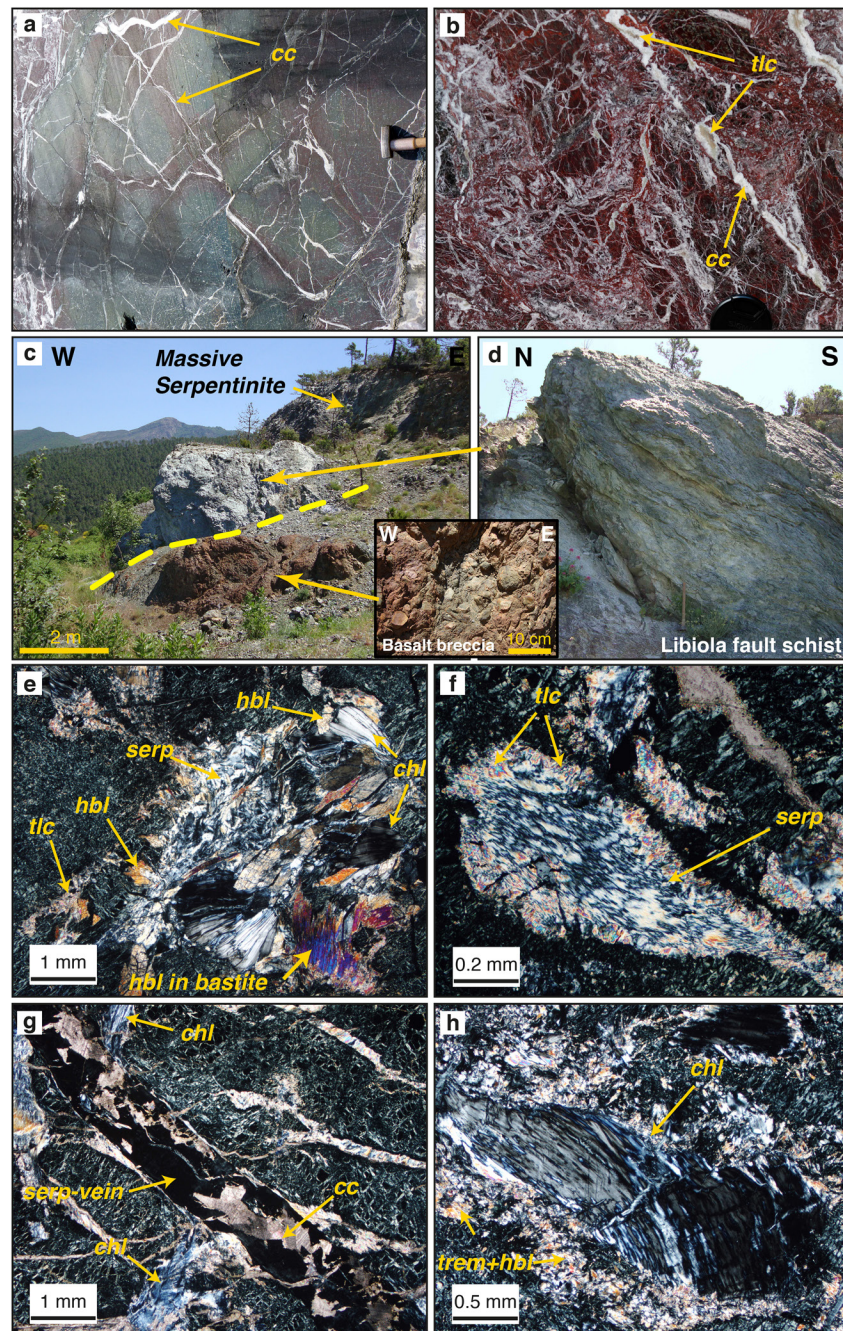


Figure 2. (a) Strongly veined and partly oxidized green opicalcite with oxidation initiating along calcite veins. (b) Highly oxidized, red opicalcite characterized by intense fracturing and brecciation, showing crosscutting relationships of multiple generations of calcite-veins and talc in druses. (c and d) Lens of tremolite-rich fault schist at the contact between massive serpentinites and brecciated pillow basalts at the Libiola mining site (LLB) (e–h) Microphotographs of replacement textures in green opicalcites using crossed polarized light: (e) Chlorite-amphibole-vein with fan-shaped chlorite, serpentine, amphibole blades (hornblende to actinolite-hornblende), and fine-grained talc at the vein rim. (f) Fibrous serpentine in a bastite replacing pyroxene with talc forming a rim around bastite. (g) Late serpentine-vein with fragments of calcite formed by reactivation of an older calcite-vein that cuts the serpentine mesh texture. (h) Chlorite replacing pyroxene in a bastite with fine-grained tremolite and hornblende forming a rim around bastite. Abbreviations: cc–calcite; chl–chlorite; hbl–hornblende; serp–serpentine; tlc–talc; trem–tremolite.

oxidation from bottom to top of the exposed sequence. A transect through all three lithologies was sampled to account for variations in veining and oxidation.

Serpentinites and tremolite-schists from the Val Graveglia Unit were sampled at one abandoned mining site close to the village of Libiola. In the study area, the serpentinites over-thrust the brecciated basalts and are therefore not associated with the underlying stockwork deposits. A prominent lens of tremolite-schist at the contact between the serpentinites and the brecciated basalts was sampled as well (Figures 2c and 2d) (from here on referred to as Libiola fault schists). In addition, gabbro samples from the Bracco Unit investigated by Molli (1995) were used in this study for strontium isotope analyses.

3. Analytical Procedures

3.1. Petrographic Characterization

The mineralogy and petrology were investigated on thin sections with transmitted light microscopy and using a JEOL JSM-6390 LA scanning electron microscope with energy dispersive X-ray spectroscopy capabilities. Quantitative element concentrations were obtained by electron microprobe analysis carried out on a JEOL JXA-8200 at ETH Zurich. The beam was set to 15 kV accelerating potential, 1–10 μm beam size, and 5–20 nA beam current. Natural and synthetic standards were used for calibration. Additionally, X-ray diffraction (XRD) spectra were acquired on vein powders with a LynxEye X-ray diffractometer (Bruker AXS D8 Advance) at ETH Zurich to determine the carbonate mineralogy.

3.2. Major and Trace Element Analysis

Bulk rock powders of the serpentinites and opicalcites were prepared by cutting away the outermost rind to remove contamination, crushing in a steel mortar, and grinding to a powder in an agate mill. Major and trace element analysis of the powders were obtained by Panalytical Axios wave-length dispersive X-ray fluorescence spectrometry (WD-XRF, 2.4 kV) at ETH Zurich after fusing the bulk rock powders to glass beads with Lithium-Tetraborate (ratio 1:5). Bulk rock trace element compositions were measured on glass beads with a laser-ablation micro-sampler coupled to an inductively coupled Elan 6000 plasma mass spectrometer (LA-ICP-MS). Boron and REE concentrations in ultramafic rocks were determined at the commercial Activation Laboratories Ltd. (Ancaster, Canada) by PGNAA Elemental Analyzer and by using its research quality Lithium Metaborate/Tetraborate Fusion ICP-MS method, respectively. Mineral REE compositions were measured on thin sections with a Resonetics Resolution 155 laser ablation system, coupled to a Thermo Element XR Sectorfield ICP-MS and using a diameter of 20–40 μm . Data reduction was performed using the Matlab-based code SILLS (Guillong et al., 2008).

3.3. Strontium Isotope Analyses

To prepare whole-rock powders of gabbros and ultramafic rocks for isotope analysis, rock samples were cut, separated from major calcite veins, crushed in a steel mortar, and ground in an agate mill. Strontium isotope analyses were performed on a Thermo Finnigan Neptune 53 MC-ICP-MS at ETH Zurich, after dissolution in a mixture of HF and HNO₃ according to ion exchange procedures developed by de Souza et al. (2010) and Deniel and Pin (2001). Because of the highly heterogeneous carbon content, the carbonate-rich green and red opicalcites were decarbonized at least twice (to ensure complete carbonate removal) with 2M HCl prior to dissolution and the final residues were analyzed with a coulometer to determine if all carbonate had been dissolved (Vogel, 2016).

Calcite veins were micro-drilled to extract different vein generations and were dissolved with the following procedure: carbonate powders were dissolved in concentrated HCl, dried down, re-dissolved in concentrated HNO₃, dried down and diluted 150 times with 2% HNO₃ prior to analysis. The long-term average value for $^{87}\text{Sr}/^{86}\text{Sr}$ of the NBS987 standard measured during the period of analysis is 0.710243 with a 2σ standard deviation of 21 $\mu\text{g/g}$ ($N = 43$). The $^{87}\text{Sr}/^{86}\text{Sr}$ ratios were adjusted for mass bias by normalizing to a $^{87}\text{Sr}/^{86}\text{Sr}$ ratio of 0.1194 and are reported relative to the certified value of $^{87}\text{Sr}/^{86}\text{Sr} = 0.71024$ for the NBS987 standard. In addition, the $^{87}\text{Sr}/^{86}\text{Sr}$ ratios have been corrected for their age by using the measured Rb/Sr to an average age of 160 Ma (Jurassic).

3.4. Stable Isotope Analyses

Hydrogen and oxygen isotope analyses of silicates were carried out on bulk rock powders of the serpentinites and green opihicalcites. Hydrogen isotope (δD) compositions were analyzed using the high-temperature (1,400°C) reduction method with He as a carrier gas and a TC-EA (Flash1112HT, Thermo Fisher) interfaced to a Delta Plus XP IRMS at IGG-CNR, Pisa (Italy). Oxygen isotope values were determined on whole-rock powders after decarbonization of all the samples with 2M HCl (see Section 3.3). Measurements were conducted at the Institute of Earth Sciences at the University of Lausanne (Switzerland) using a CO₂ laser fluorination system coupled to a Finnigan MAT-253 mass spectrometer. Results are given in standard δ -notation, expressed relative to the Vienna Standard Mean Ocean Water (V-SMOW) in permil (‰). Replicate hydrogen isotope analyses of internal standards give an average precision better than $\pm 5\%$. Oxygen analyses were duplicated or triplicated and corrected to the LS-1 in house standard, which yielded an average value of $18.1 \pm 0.6\%$. However, typical precision for the standard analyses is $\pm 0.2\%$. Higher errors during analysis were likely caused by oxidation during fluorination of the fine-grained powders, leading to higher background interferences.

Oxygen and carbon isotope analyses of micro-drilled calcite veins were analyzed on a GasBench II with a continuous-flow IRMS setup, after the method of Breitenbach and Bernasconi (2011). Isotope ratios are reported in permil (‰) using the conventional δ -notation and with respect to the V-SMOW for oxygen and Vienna Pee Dee Belemnite (V-PDB) for carbon. Standard deviation was 0.05‰ for both $\delta^{13}C$ and $\delta^{18}O$.

4. Results

4.1. Sample Description

Macroscopic and microscopic investigation of the serpentinites, and green and red opihicalcites indicate a similar protolith but highly variable alteration characteristics. The serpentinites from the basement of the Bracco Unit are completely serpentinitized harzburgites and clinopyroxene-poor lherzolites. The serpentinites and opihicalcites show a typical mesh texture with no relicts of primary minerals except for Cr-rich spinel, which is a common magmatic mineral in peridotites and is strongly altered, as well as rare diopsidic and partly serpentinitized clinopyroxene that is also most likely of primary magmatic origin. The groundmass of the opihicalcites commonly contains talc and chlorite as microscopic intergrowths in the serpentine mesh and amphibole either around bastites that replace orthopyroxene or forming veins (Figure 2). Oxidation is observed in both green and red opihicalcites. In the green opihicalcites, oxidation of the serpentine mesh texture initiates along calcite veins locally producing a reddish halo along the veins (Figure 2a). In contrast, the red opihicalcites show pervasive oxidation of the groundmass as defined by the high abundance of hematite (as determined by polarization microscopy) and/or other Fe-oxides and -hydroxides finely dispersed in the groundmass, which gives the intense red color (Figure 2b). Similarly, calcite veining is significantly more abundant in the red opihicalcites, where calcite veins mostly follow mm to cm wide fractures. In the red opihicalcites, numerous generations of calcite veins can be distinguished based on fabrics and crosscutting relationships (Figure 3): (1) Early calcite veins, in long planar fractures and locally including fragments of serpentine fibers; (2) Thinner ribbon calcite veins as bands of subparallel calcite veins that commonly show extensional structures; (3) Vein networks including jigsaw puzzle breccias, consisting of a disarray of calcite veinlets with complex geometry and a clear hydrofracture texture; (4) Breccias with pink/gray calcite-micrite matrix and serpentinite clasts; and (5) Late-stage calcite veins filling thick and branching irregular fractures. These latter veins cut across older features and reactivate older surfaces. Furthermore, late-stage calcite veins are associated with talc druses in the center of the veins, as previously reported in detail by B. Treves et al. (1995).

The Cava dei Marmi fault schists are strongly sheared, highly heterogeneous, and characterized by the abundance of talc, tremolite, and calcite. Serpentine occurs as rare clasts and chlorite in pockets. Such assemblages are typical for metasomatic rocks observed in detachment fault zones on the seafloor and suggests an ocean floor setting (Boschi et al., 2006a, 2006b; Karson et al., 2006). However, tectonic reworking during the Alpine orogenesis cannot be excluded completely.

Mg-rich gabbros, sampled in the Bracco Pass and the Bonassola area, intrude the serpentinites in the Bracco Massif and commonly show medium- to coarse-grained porphyroblastic textures, consisting mainly of

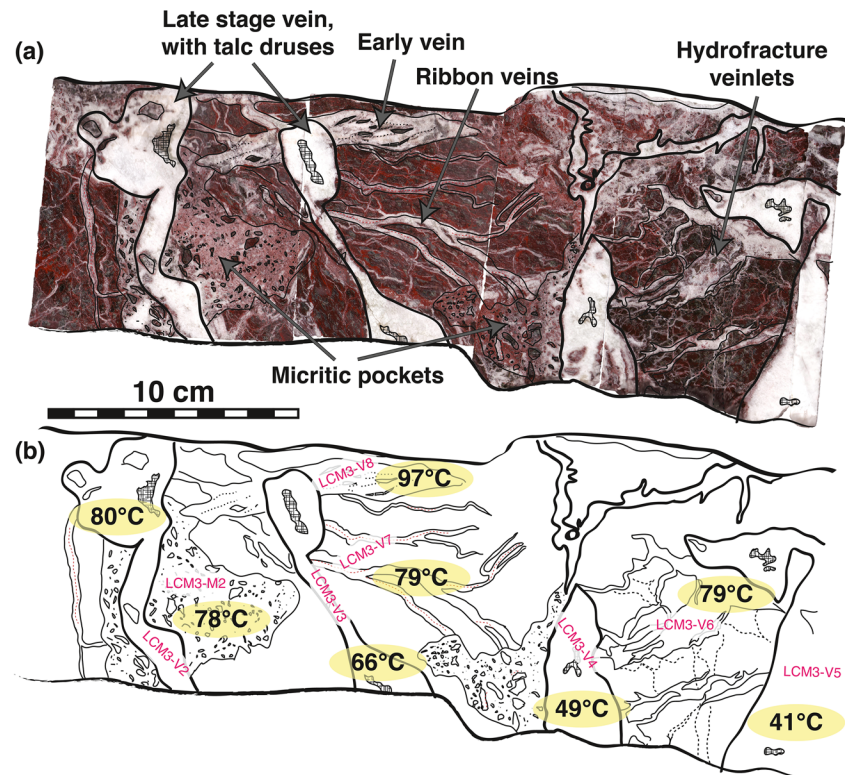


Figure 3. Rock slab of a red opihcalcite from Cava dei Marmi showing (a) crosscutting relationships between different vein generations: (1) early calcite veins, (2) thinner ribbon veins, (3) vein networks with clear hydrofracture texture (hydrofracture veinlets), (4) micritic calcite matrix, and (5) late calcite veins (see text for more details). (b) Temperature variations (yellow ellipses) calculated from $\delta^{18}\text{O}_{\text{carb}}$ values of different micro-drilled veins.

clinopyroxene and plagioclase. High temperature shear zones are preserved within sections of undeformed gabbros. In the Bonassola area the effect of hydrothermal circulation in the gabbros is also apparent. Wide-spread fractures filled with Mg-hornblende (\pm plagioclase), which replaces the clinopyroxene, occur as parallel swarms crosscutting the high-T shear zones. For a detailed description of the gabbros, we refer to Molli (1995) and Tribuzio, Renna, et al. (2014).

Macro- and microscopically, the Val Graveglia serpentinites are similar to the Bracco serpentinites with a dominance of serpentine and magnetite and no primary mineral phases preserved other than spinel. Sulfide minerals, amphibole, and talc are rare in these serpentinites. Only the Libiola fault schists are characterized by an abundance of elongated tremolite crystals and are randomly crosscut by tremolite veins, whereas serpentine is rare and only present as angular clasts. Chlorite is visible in pockets, which are locally crosscut by tremolite veins.

4.2. Mineralogy and Mineral Chemistry

4.2.1. Serpentine, Talc and Chlorite

The texture and chemical composition of serpentine strongly depends on the primary mineral phases it replaces. Serpentine after olivine is the main phase forming the groundmass and commonly develops a mesh or ribbon texture. The meshes typically are formed by fibrous serpentine at the rims and very fine-grained, homogeneous, and locally isotropic serpentine in the mesh cores suggesting a dominance of lizardite and chrysotile. Orthopyroxene has been completely replaced by aggregates of fibrous serpentine minerals that retain the prismatic shape of the original orthopyroxene grains and form bastites. In some of the opihcalcites, serpentine veins cut the mesh texture and were reactivated by calcite veining or vice versa (Figure 2g). No evidence of serpentine recrystallization was observed that would indicate a regional metamorphic

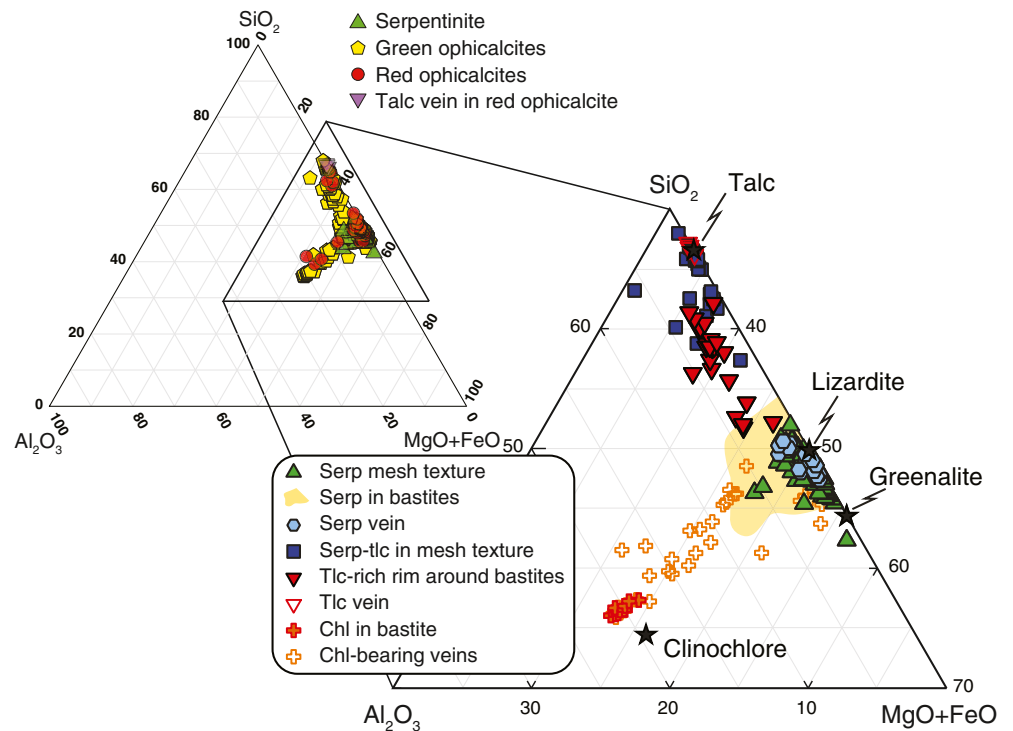


Figure 4. Ternary diagram of SiO_2 -($\text{MgO} + \text{FeO}$)- Al_2O_3 showing chemical compositions of serpentine (mesh rim, mesh cores, veins, bastite), chlorite, and talc from serpentinites, green and red opicalcites (see top left). Note, several analyses represent fine-grained mineral intergrowths of serpentine with talc or chlorite, not resolvable by EMP analysis. Stars represent endmember compositions for lizardite, greenalite, clinocllore, and talc. Yellow area represents serpentine in bastites.

overprint, which is consistent with maximum metamorphic conditions around prehnite-pumpellyite facies as constrained by Garuti et al. (2008).

The chemical variation of serpentine (serpentine mesh texture, bastite, and veins), chlorite, and talc from serpentinites and opicalcites is presented in Figure 4. In the serpentinites, only serpentine with compositions very close to lizardite was analyzed and no talc or chlorite was detected. In all samples (i.e., serpentinites, green and red opicalcites), serpentine after olivine shows a large variation in Mg\# ($\text{Mg}/(\text{Mg} + \text{Fe})$) of 0.76–0.89, whereas bastites have a narrower range (0.81–0.93). Mesh cores have lower Mg\# than mesh rims, indicating an enrichment in FeO_{tot} from rim to core of the serpentine meshes with up to 9.8 wt.% FeO_{tot} in mesh cores (with no magnetite present). Bastites have highly variable compositions within individual grains and show higher contents of Cr_2O_3 and Al_2O_3 , and low contents of NiO compared to mesh serpentine, reflecting the primary orthopyroxene composition (see Table S2). Serpentine veins are generally poorer in FeO_{tot} compared to groundmass serpentine.

Mineral assemblages with talc and chlorite were only detected and analyzed in the opicalcites. In addition, mixing trends between serpentine and chlorite, and between serpentine and talc suggest fine-grained mineral intergrowths on a submicrometer scale (Figure 4). Polarization microscopy indicates that talc occurs in pockets in the core of the serpentine mesh texture, as fine-grained rims around bastites, and intergrown within serpentine in the bastites (Figures 2e and 2f). It is also present as fine intergrowths with amphibole and chlorite forming veins. In some red opicalcites, coarse-grained talc-druses (up to 3 cm wide) occur in late-stage calcite veins (Figures 2b and 3). In the Cava dei Marmi fault schists that border the opicalcites, talc occurs as fine-grained aggregates in pockets and, rarely, within the cores of serpentine meshes. Only analyses of talc veins (within calcite veins) from the red opicalcite yielded pure talc analyses, whereas all other occurrences are fine serpentine-talc intergrowths. Chlorite forms either fan-shaped aggregates in the serpentine groundmass, where it occurs with talc and amphibole as vein-like features, or replaces pyroxene

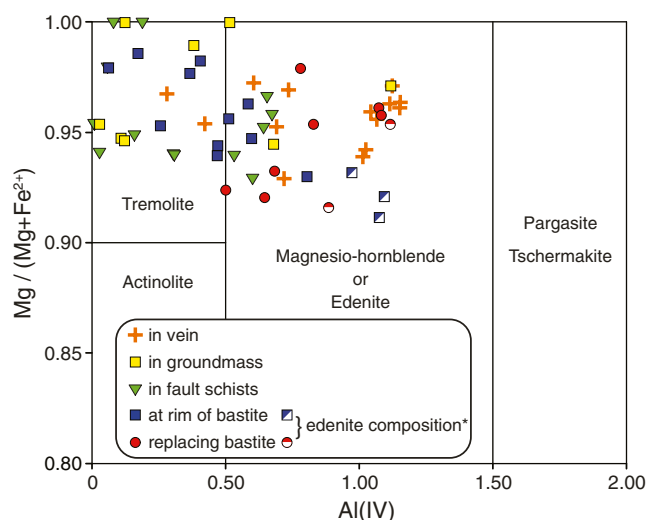


Figure 5. Amphibole classification after Leake et al. (1997) showing variable compositions in veins, rims around bastite, in fault rocks and in the groundmass. Atoms are calculated as 23 oxygens. $Al(IV) = 8 - Si$. $(Na + K)_{[A]} \geq 0.50$ for edenite (marked with *) and $(Na + K)_{[A]} \leq 0.5$ for magnesio-hornblende.

in bastites (Figures 2g and 2h). In most cases, chlorite forms fine-grained intergrowths with serpentine (Figure 4). In addition, chlorite is associated with altered Cr-rich spinel in the serpentinites and ophicalcites.

4.2.2. Amphibole

Amphiboles are present mostly in the ophicalcites and in the Cava dei Marini and Libiola fault schists. They are colorless, calcic in composition, and form needles and blades at the rim of bastites or partly replacing bastites. They are also found as veins and in pockets, or in the serpentine mesh texture as very fine intergrowths with serpentine, talc, and chlorite (Figures 2e and 2h). In the fault schists, amphiboles are present as veins or in pockets together with chlorite. Following the classifications of Leake et al. (1997), the amphiboles are mostly magnesio-hornblende with lesser tremolites (Figure 5) and show no clear distinction between occurrences in veins and the fault schists. However, the chemical compositions of the amphiboles that form rims around bastites and those that replace bastites are more variable and also include edenite compositions.

4.2.3. Calcite Veins

The ophicalcites have a complex network of multiple generations of veins, ranging in size from a mm-scale microscopic network that appears to hydrofracture the mesh texture, to macroscopic veins that are several centimeters thick and several meters in length. The veins are composed mainly of calcite as previously also determined by Schwarzenbach, Früh-Green, Bernasconi, Alt, and Plas (2013). No aragonite, Mg-calcite or dolomite were detected by XRD or microscopic observations, although B. E. Treves and Harper (1994) described calcite fibers and rosettes that may represent pseudomorphs of former aragonite crystals. Locally, calcite is present in the core of the serpentine meshes.

4.2.4. Minor Phases and Oxides

All magnetite is most likely of secondary origin associated with serpentinization and carbonation. Very small magnetite grains and oxide needles are distributed homogeneously in the serpentinite mesh texture or form thick oxide bands at the rim of serpentine veins as observed by polarization microscopy. Magnetite also occurs locally as euhedral crystals in calcite and serpentine veins. Hematite, Fe-oxides and/or Fe-hydroxides give the noticeable red color in the red ophicalcites and occur along calcite veins in the green ophicalcites. In some cases, ghost-structures of hematite in calcite veins can be found, reflecting older serpentine mesh structures. Almost no magnetite could be observed in the bastites.

Cr-rich spinel is observed in all thin sections and shows incipient alteration to Fe-chromite \pm chlorite along the edges. The composition of Cr-spinel varies strongly between the different samples: Cr_2O_3 -contents range from 25.8 to 38.1 wt.%, MgO-contents are between 7.8 and 17.5 wt.% and Al_2O_3 -contents are between 18.9 and 39.0 wt.%. Sulfide minerals are abundant in calcite veins and occur locally within the serpentine mesh. Sulfides include pentlandite, pyrrhotite, pyrite, millerite, siegenite and rare chalcopyrite, and are described in detail by Schwarzenbach, Früh-Green, Bernasconi, Alt, Shanks III, et al. (2012).

4.3. Bulk Rock Major and Trace Element Geochemistry

Bulk rock major element compositions of serpentinites and ophicalcites are plotted (on an anhydrous basis) in Figure 6 together with serpentinites and talc-amphibole schists from the AM (Boschi et al., 2006a) and fresh peridotites from the Internal Ligurian units (Mt. Fucina; Rampone et al., 1996). The chemical composition of the serpentinites overlaps with the serpentinites from the AM and with the Internal Ligurian peridotites; however, our samples on average show high Fe_2O_3 and higher Al_2O_3 contents compared to the AM serpentinites. The gradual transition from serpentinite to ophicalcite from the Bracco Unit is highlighted by an increase in CaO (up to 6.4 wt.%), due to carbonate veining, and by an increase in SiO_2 and a decrease in MgO, due to the formation of amphibole/talc. A similar trend is found for the AM talc schists, especially with regard to SiO_2 and MgO contents.

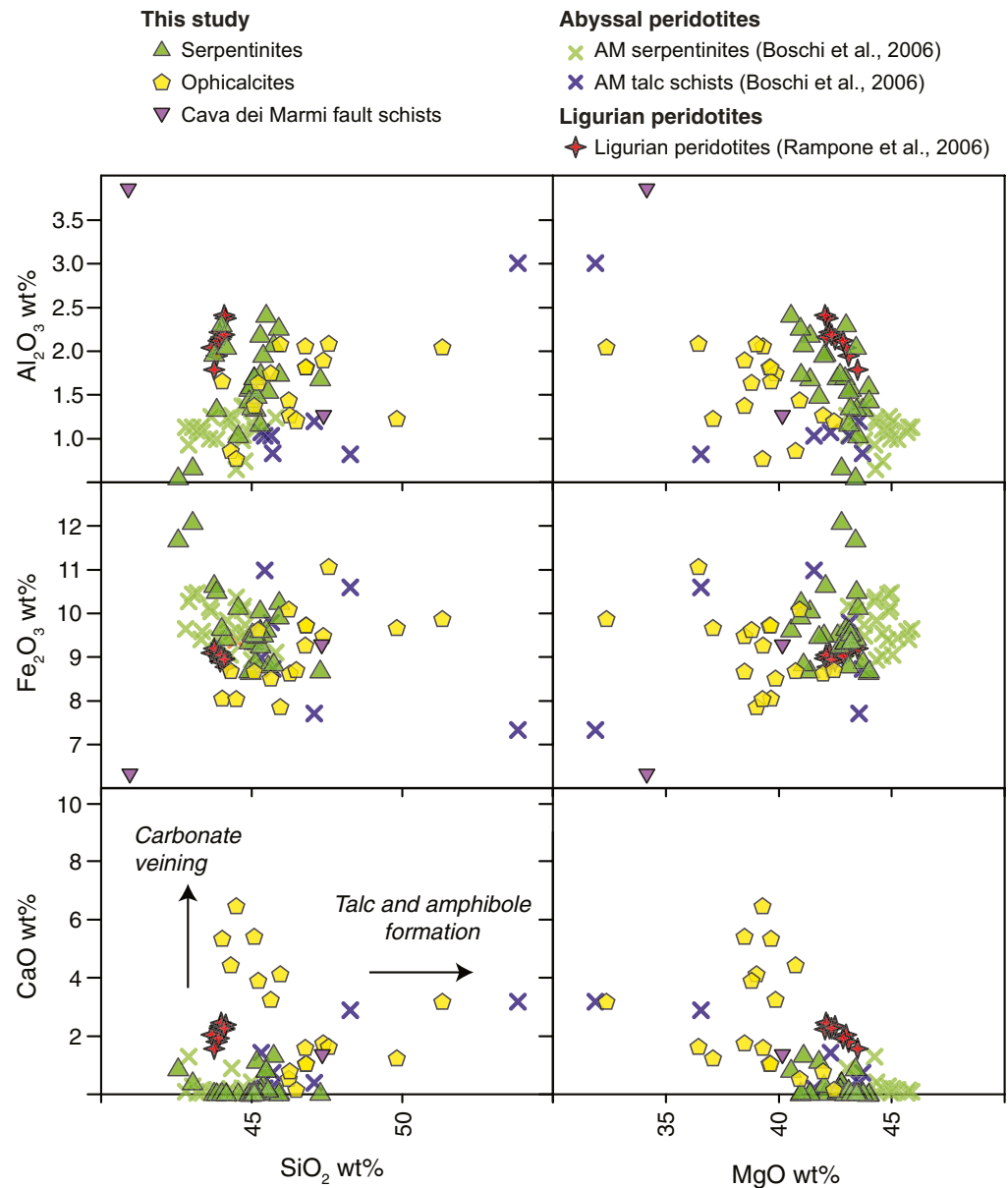


Figure 6. Harker-type diagrams showing the chemical variation of selected major elements (on anhydrous basis) of the Bracco serpentinites, ophicalcites and fault rocks compared to other Ligurian peridotites (Rampone et al., 1996), the Atlantis Massif serpentinites (AM serpentinites) and talc-amphibole schists (AM talc schists) (Boschi et al., 2006a). Total iron calculated as ferrous iron. The ophicalcites are generally enriched in SiO_2 , Al_2O_3 , and CaO , and depleted in MgO compared to basement serpentinites reflecting formation of talc, amphibole, and calcite, the latter in veins.

Trace element patterns reveal typical enrichments in fluid mobile elements (FMEs) particularly Cs, Sr, and U (Figures 7a and S1). On average, Cs, Rb, and Sr are more enriched in the ophicalcites than in the basement serpentinites. Ba concentrations of basement serpentinites show both enrichment and depletion compared to the primitive mantle. The ophicalcites have intermediate Ba compositions. Overall, the serpentinites from the Bracco Unit overlap with the trace element patterns found in serpentinites from the AM. Metals (e.g., Cu, Zn) show similar concentrations in the serpentinites and ophicalcites.

Bulk rock REE patterns of the serpentinites and ophicalcites are characterized by variable LREE enrichments and a nearly flat pattern of the HREE (Figure 7b). The serpentinites and the ophicalcites mostly have overlapping bulk rock REE patterns. However, the ophicalcites have a smaller range of HREE

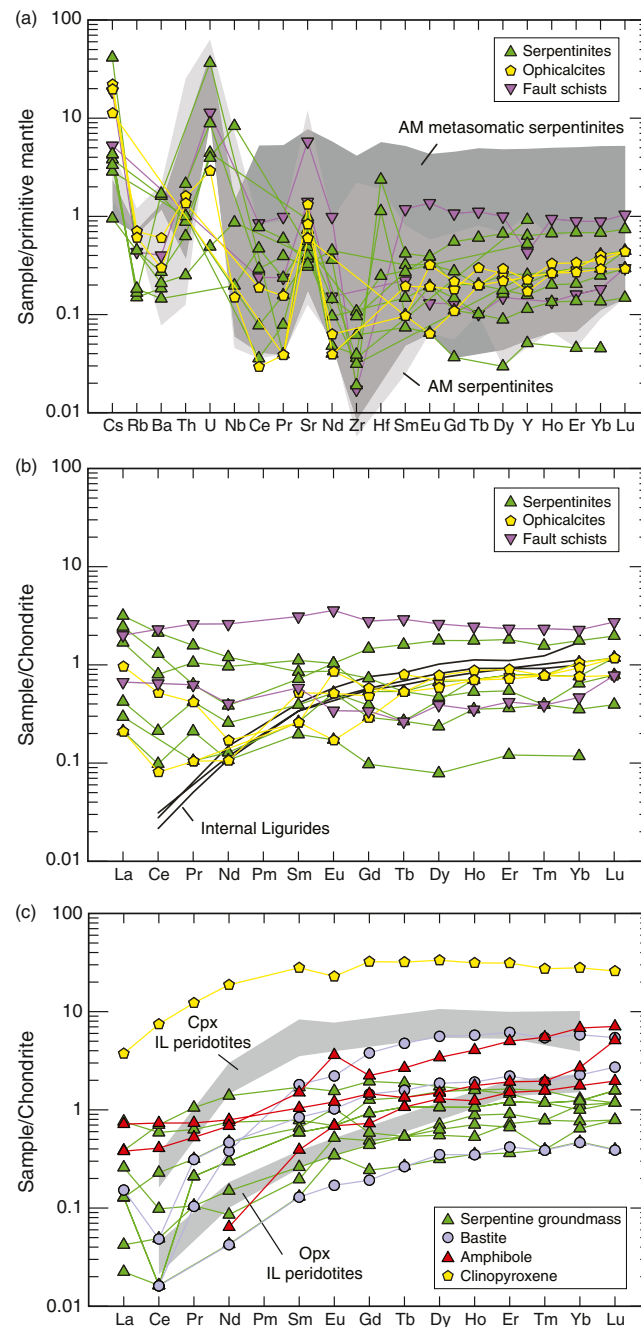


Figure 7. (a) Spider diagram showing trace element variations of selected bulk rock serpentinites, ophicalcites, and Cava dei Marmi fault schists normalized to primitive mantle (after McDonough & Sun, 1995). Atlantis Massif serpentinites (light gray field) and metasomatic serpentinites (dark gray field) are shown for comparison (data from Boschi et al., 2006a). Noticeable are enrichments in Fluid Mobile Elements (FME) particularly Cs, U, and Sr. (b) Chondrite-normalized REE pattern (after Sun & McDonough, 1989) of selected bulk rock serpentinites, ophicalcites, and Cava dei Marmi fault schists. Peridotite REE compositions from Internal Liguride (IL) Units are plotted for comparison (Rampone et al., 1996). Serpentinites and ophicalcites have a relatively flat REE pattern and elevated LREE compositions compared to unaltered IL peridotites. (c) Chondrite-normalized REE concentration patterns (after Sun & McDonough, 1989) determined in situ on minerals from ophicalcites and fault schists. Orthopyroxenes (Opx) and clinopyroxenes (Cpx) of the Internal Liguride Peridotites (IL) from fresh clinopyroxene-poor lherzolites are plotted for comparison (Rampone et al., 1996).

concentrations than the serpentinites and tend to have lower average LREE concentrations. In comparison to the peridotites from the Internal Liguride Units (Rampone et al., 1996), the studied serpentinites and ophicalcites are enriched in LREE.

In situ mineral analyses of the mesh serpentine and bastite minerals yielded different REE patterns than the serpentinite bulk rock analyses (Figure 7c). They are characterized by highly variable and depleted LREE compositions and a nearly flat pattern for the HREE. Both groundmass serpentine and bastites display slight positive Eu anomalies, but variable (positive and negative) Ce anomalies. Some of the bastites have slightly higher REE compositions than the serpentine groundmass and reflect the precursor pyroxene: LREE depletion, and a flat HREE pattern. One analysis of clinopyroxene yielded elevated REE compositions compared to the bastites and serpentines.

4.4. Isotope Compositions

4.4.1. Bulk Rock Isotope Systematics

The $\delta^{18}\text{O}$ values of the serpentinites and ophicalcites in the Bracco Unit range between 6.2 and 7.5‰. The Cava dei Marmi fault schists—dominated by talc and tremolite—have the highest value with 14.7‰. The serpentinites and Libiola fault schists from the Val Graveglia Unit yield $\delta^{18}\text{O}$ values of 8.6 and 5.1‰, respectively (Table 1).

The average δD values of the ophicalcites is slightly higher ($\delta\text{D} = -68 \pm 6\text{‰}$) than the serpentinites ($\delta\text{D} = -74 \pm 6\text{‰}$), whereas the Cava dei Marmi fault schists have values of $\delta\text{D} = -75$ and -59‰ . With the exception of the Libiola fault schist that has a δD value of -40‰ , the serpentinites from the Val Graveglia Unit are similar to the Bracco Unit with an average δD value of $-76 \pm 2\text{‰}$ (Table 1).

In addition to the serpentinites and ophicalcites, gabbros from the Bracco unit were analyzed for their Sr isotope composition. Overall, the studied samples have a large range in $^{87}\text{Sr}/^{86}\text{Sr}$ ratios (Figure 8). The gabbros have the lowest $^{87}\text{Sr}/^{86}\text{Sr}$ ratios and range from 0.70295 to 0.70457; these values are close to depleted MORB mantle compositions (0.7025; Rehkämper & Hofmann, 1997) but also show moderate exchange with seawater-derived hydrothermal fluids. The (decarbonated) ophicalcites and the Cava dei Marmi fault schists have similar $^{87}\text{Sr}/^{86}\text{Sr}$ ratios and display values between the gabbros and Jurassic seawater (0.7068–0.7070 for 165–160 Ma; Wierzbowski et al., 2017). The micro-drilled carbonate veins have a range in $^{87}\text{Sr}/^{86}\text{Sr}$ ratios of 0.70503–0.70718, which are mostly lower than Jurassic seawater compositions but on average higher than the ophicalcites. Remarkable is the fact that the Bracco serpentinites have $^{87}\text{Sr}/^{86}\text{Sr}$ ratios ranging from 0.70337 to 0.70857, whereby most serpentinites display $^{87}\text{Sr}/^{86}\text{Sr}$ ratios higher than Jurassic seawater. The $^{87}\text{Sr}/^{86}\text{Sr}$ ratios of the Val Graveglia serpentinites are comparably high with values of 0.70703–0.70864, and the Libiola fault schist has the highest value of 0.71400.

4.4.2. Carbon and Oxygen Isotope Systematics of Calcite Veins

The carbonate veins have $\delta^{13}\text{C}$ values of 1.1–3.0‰ (V-PDB) (Figure 9a). The $\delta^{18}\text{O}$ values range from 15.4 to 24.6‰ (V-SMOW) and record variations in precipitation temperatures (Figures 3 and 9b, Table S4). Calcite precipitation temperatures were calculated using the calcite-water fractionation equation of Friedman and O'Neil (1977) assuming an initial seawater composition of $\delta^{18}\text{O} = -1\text{‰}$ for an ice-free Earth. This yields an overall trend of decreasing temperature from 108°C in the early and ribbon calcite veins to 41°C in the late stage calcite veins. These temperatures agree with results of Schwarzenbach, Früh-Green, Bernasconi, Alt, & Plas (2013) that showed a decrease with age from 151°C to 49°C. This trend is associated with early calcite veins with the lowest $\delta^{13}\text{C}$ values ($\approx 1\text{‰}$) and $^{87}\text{Sr}/^{86}\text{Sr}$ ratios close to seawater composition, and late calcite veins with $\delta^{13}\text{C}$ values of 2–3‰ and lower $^{87}\text{Sr}/^{86}\text{Sr}$ ratios (Figure 9a).

5. Discussion

5.1. Alteration History Based on Microstructures

The mineralogical and geochemical characteristics of the studied serpentinites indicate a multiphase alteration process with infiltration of fluids along passive tension fractures and locally focused along fault zones. The chemical zoning of the mesh-texture serpentine after olivine (i.e., Fe-poor rim vs. Fe-rich core)

Table 1
Sample Location, Oxygen, Hydrogen, and Strontium Isotope Compositions

Sample	Rock type	Location	Coordinates		Sr (μg/g)	⁸⁷ Sr/ ⁸⁶ Sr	2	δD	δ ¹⁸ O (‰, V-SMOW)	‰ stdv
							Standard error			
Bracco Unit			N	E						
LBR5	Serpentinite	Bonassola outcrop (close to Rodingite)	44°10'32"	09°35'08"	19	0.703370	0.000039			
LCA4	Serpentinite	Carro old mining site	44°16'41"	09°35'26"	4			−74		
LCA5	Serpentinite	Carro old mining site	44°16'41"	09°35'26"	5			−71		
LCA6A	Serpentinite	Carro old mining site	44°16'41"	09°35'26"	6			−68		
LCA7	Serpentinite	Carro old mining site	44°16'41"	09°35'26"	5			−67		
LCG10	Serpentinite	Cava Galli	44°10'28"	09°36'22"	6	0.708481	0.000022	−73		
LCG11	Serpentinite	Cava Galli	44°10'28"	09°36'22"	7	0.708154	0.000026	−67	7.3	0.2
LCG9	Serpentinite	Cava Galli	44°10'28"	09°36'22"	7			−72		
LCM18	Serpentinite	Cava dei Marmi	44°11'51"	09°35'20"	8	0.707849	0.000025	−77		
LCM21	Serpentinite	Cava dei Marmi	44°11'51"	09°35'20"	6	0.707867	0.000022	−86		
LCP12	Serpentinite	Cava Piazza	44°13'52"	09°32'59"	9	0.708154	0.000026			
LPM1	Serpentinite	Punta dei Marmi	44°11'53"	09°33'39"	11	0.703510	0.000022			
LSP10	Serpentinite	Along road cut on SS332	44°13'06"	09°35'16"	9	0.708578	0.000026	−78	7.5	0.5
LSP11	Serpentinite	Along road cut on SS332	44°13'45"	09°35'21"	15	0.707940	0.000016	−81		
LSP12	Serpentinite	Along road cut on SS332	44°13'45"	09°35'21"	11			−81		
LSP3	Serpentinite	Along road cut on SS332	44°12'35"	09°35'26"	11	0.706650	0.000044	−68		
LA1	Green opicalcite	Cava dei Marmi	44°11'51"	09°35'20"	27	0.705589	0.000022			
LA3a ^a	Green opicalcite	Cava dei Marmi	44°11'51"	09°35'20"				−71		
LA9 ^a	Green opicalcite	Cava dei Marmi	44°11'51"	09°35'20"	44	0.705456	0.000028	−74	7.0	0.1
LA12 ^a	Green opicalcite	Cava dei Marmi	44°11'51"	09°35'20"	13	0.705732	0.000036	−63	6.2	0.3
LA14 ^a	Green opicalcite	Cava dei Marmi	44°11'51"	09°35'20"				−65		
LA15 ^a	Green opicalcite	Cava dei Marmi	44°11'51"	09°35'20"				−77		
LA16 ^a	Green opicalcite	Cava dei Marmi	44°11'51"	09°35'20"	17	0.705129	0.000031	−67		
LCG3	Green opicalcite	Cava Galli	44°10'28"	09°36'22"	11	0.705770	0.000027	−63		
LCM6	Cava dei Marmi fault schist (Serp- Talc-Trem Schist)	Cava dei Marmi	44°11'51"	09°35'20"	114	0.705501	0.000034	−59		
LCM7	Cava dei Marmi fault schist (Serp- Talc Schist)	Cava dei Marmi	44°11'51"	09°35'20"	28	0.705779	0.000036	−75	14.8	0.3
LCM2	Red opicalcite	Cava dei Marmi	44°11'51"	09°35'20"	22	0.705419	0.000016			
LCM3	Red opicalcite	Cava dei Marmi	44°11'51"	09°35'20"	14	0.704896	0.000033			
LCG4	Red opicalcite	Cava Galli	44°10'28"	09°36'22"	12	0.705753	0.000016			
LCG5	Red opicalcite	Cava Galli	44°10'28"	09°36'22"	11	0.705995	0.000030			
G61 ^b	Banded metagabbro	Bracco Pass	n.r.		222	0.703355	0.000028			
G28 ^b	Banded metagabbro	Bracco Pass	n.r.		204	0.703789	0.000023			
G29 ^b	Banded metagabbro	Bracco Pass	n.r.		185	0.702956	0.000027			
GC2f ^b	Gabbro	Bracco Pass	n.r.		249	0.704079	0.000022			
G22 ^b	Gabbro	Bracco Pass	n.r.		253	0.703995	0.000021			
LCC2	Gabbro	Castagnola	44°13'51"	09°34'57"	201	0.704574	0.000039			
LCC5	Gabbro	Castagnola	44°13'51"	09°34'57"	190	0.704509	0.000039			
GC1 ^b	Gabbro	Bracco Pass	n.r.		279	0.704246	0.000021			

Table 1
Continued

Sample	Rock type	Location	Coordinates	Sr ($\mu\text{g/g}$)	$^{87}\text{Sr}/^{86}\text{Sr}$	² Standard error	δD	$\delta^{18}\text{O}$ (‰, V-SMOW)	‰ stdv
LPB6	Mylonitic metagabbro	Bracco Pass	n.r.	266	0.703507	0.000039			
LBR13	Mylonitic metagabbro	Bonassola	44°10'49" 09°35'04"	219	0.703370	0.000039			
LBR11	Mylonitic metagabbro	Bonassola	44°10'49" 09°35'04"	185	0.703470	0.000039			
G18ab ^b	Porphyroclastic metagabbro mylonites	Bracco Pass	n.r.	185	0.703551	0.000024			
G19 ^b	Porphyroclastic metagabbro mylonites	Bracco Pass	n.r.	225	0.703907	0.000022			
G7 ^b	Porphyroclastic metagabbro mylonites	Bracco Pass	n.r.	231	0.702991	0.000022			
GC11 ^b	Porphyroclastic metagabbro mylonites	Bracco Pass	n.r.	286	0.704216	0.000022			
<i>Val Graveglia Unit</i>									
LLB16	Serpentinite	Libiola old mining site	44°18'13" 09°26'58"	8	0.707509	0.000025	−78		
LLB17	Serpentinite	Libiola old mining site	44°18'13" 09°26'58"	7	0.707569	0.000025	−78	8.6	1.1
LLB28	Serpentinite	Libiola old mining site	44°18'13" 09°26'58"	10	0.708644	0.000024	−74		
LLB27	Serpentinite	Libiola old mining site	44°18'13" 09°26'58"	7	0.707032	0.00002			
LLB18	Libiola fault schist (mostly Trem)	Libiola old mining site	44°18'13" 09°26'58"	10			−40	5.1	0.8
LLB19	Libiola fault schist (mostly Trem)	Libiola old mining site	44°18'13" 09°26'58"	9	0.714003	0.000035			

Note. Reported Sr. n.r. = not reported; n.d. = not determined.

^aSamples from Schwarzenbach, Früh-Green, Bernasconi, Alt, Shanks III, et al., 2012, 2013, analyzed for this study. ^bSamples collected by Molli (1995) and analyzed for this study.

reflects the multistage process of serpentinization. A first stage of alteration likely resulted in the formation of Fe-rich brucite (as an intermediate phase and not preserved) and Fe-poor serpentine, which was followed by increasing H_2O - and Si-activities that resulted in progressive dissolution and replacement of olivine and Fe-rich brucite by Fe-poor serpentine and magnetite forming the magnetite-bearing veins (e.g., Beard et al., 2009; Boschi, Dini, Baneschi, et al., 2017; Schwarzenbach, Caddick, et al., 2016). A later stage of alteration is indicated by relict olivine in the core of the meshes replaced by Fe-rich serpentine, which suggests that Si-activities increased to the point where brucite and magnetite were instable (e.g., Früh-Green et al., 2004; Grozeva et al., 2017; Klein et al., 2014; Mayhew & Ellison, 2020). This interpretation is supported by local occurrences of talc in the mesh cores as well as fine-grained serpentine-talc intergrowths in the mesh texture (Figure 4). In addition to serpentinization and extensive carbonation, variations in bulk rock chemistry associated with talc, chlorite, and amphibole with highly variable compositions (Figure 6) indicate variations in fluid/rock ratios and/or fluid compositions and temperatures during progressive rock alteration (Malvoisin, 2015). Secondary amphibole and/or talc rims around bastites have been described in many oceanic serpentinites and their origins are commonly linked to early stages of mantle hydration associated with the interaction of peridotites with hydrothermal fluids during mantle upwelling (e.g., Agrinier & Girardeau, 1988; Früh-Green et al., 1996). However, in the N. Apennine serpentinites, the amphibole veins and patches cutting the serpentine mesh texture, and amphibole of hornblende to edenite composition replace bastites, which document a later stage of localized fluid infiltration likely at amphibolite-facies conditions (e.g., Schmidt, 1992). Calcite veins and talc druses filling preexisting calcite veins in the ophiolites document the final stages of serpentinite/ophicalcite alteration, whereby the abundance of talc points to late stage Si-metasomatism. These observations indicate that multiple phases of fluid-rock interaction with different fluid sources at varying temperatures have affected the N. Apennine serpentinites and ophiolites during their hydrothermal evolution.

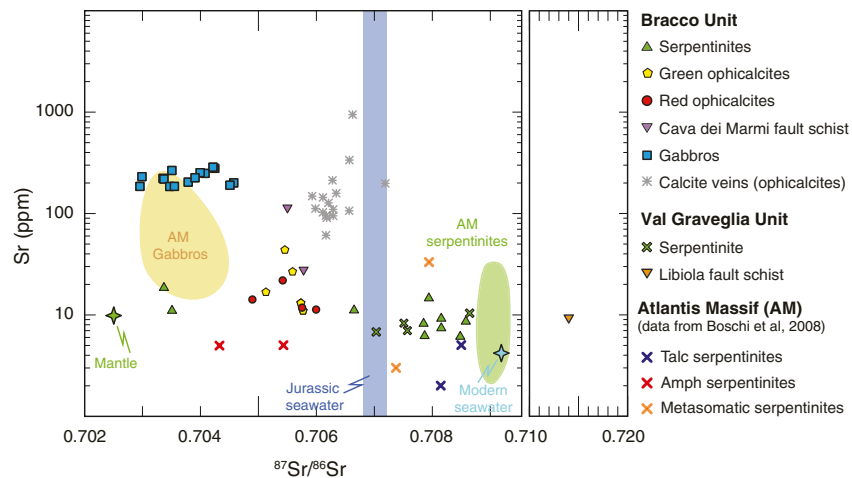


Figure 8. $^{87}\text{Sr}/^{86}\text{Sr}$ ratios vs. strontium concentrations for studied samples compared to Atlantis Massif samples (Boschi, Dini, Früh-Green, & Kelley, 2008). Mantle $^{87}\text{Sr}/^{86}\text{Sr}$ value (green star) from Rehkämper and Hofmann (1997) and $[\text{Sr}] = 9.8$ ppm from Salters and Stracke (2004) for depleted MORB mantle $^{87}\text{Sr}/^{86}\text{Sr}$ ratio for mid- to late Jurassic seawater is from Wierzbowski et al. (2017). The serpentinites generally yielded higher $^{87}\text{Sr}/^{86}\text{Sr}$ compositions than Jurassic seawater, whereas the opicalcites display lower $^{87}\text{Sr}/^{86}\text{Sr}$ ratios between Jurassic seawater and Bracco gabbros. The Libiola fault schist likely represents water-rock interaction during Alpine orogenesis.

Trace and rare Earth element patterns as well as stable and radiogenic isotope signatures provide ideal tracers for fluid sources and fluid-rock interaction processes. Importantly, major and trace element concentrations in peridotites are also modified by melting and refertilization by melt-rock interaction (Niu, 2004; Paulick et al., 2006). In the following, we first discuss the REE patterns to account for possible melt-rock interaction that could have taken place before, during or after hydrothermal alteration and then combine these observations with isotope signatures to constrain the hydrothermal alteration history and the impact of different fluid sources during serpentinization, carbonation and Si-metasomatism.

5.2. Distinguishing Melt-Rock and Fluid-Rock Interaction Processes

Melt impregnation and melting processes are typically reflected by the addition of SiO_2 , REE, and HFSE (e.g., Nb, Ta, Zr, Hf). Melt-rock interaction causes addition of LREE and HFSE to the rock in about equal proportions, whereas interaction with aqueous solutions leads to a more distinct enrichment in LREE than in HREE and HFSE (Paulick et al., 2006). In the Bracco Unit, the chondrite-normalized REE patterns of the opicalcites are similar to the basement serpentinites (Figure 7b). HREE (Gd-Lu) patterns are rather flat in both serpentinites and opicalcites, whereas the LREE (La-Eu) contents are more variable and enriched compared to the unaltered peridotites of the Internal Ligurian units (Rampone et al., 1996). Interestingly, the in situ analyses of the minerals show no LREE enrichment in the serpentinites nor the opicalcites (Figure 7c).

LREE enrichment in serpentinites compared to unaltered peridotites has been broadly documented in mid-ocean ridge serpentinites and has been associated with the mobility and incorporation of LREE in serpentinites during hydrothermal processes (Niu, 2004; Paulick et al., 2006). Records of hydrothermal processes are preserved in both the serpentine minerals and some opicalcite bulk rocks that display negative Ce anomalies in the REE patterns (Figure 7b) and have been linked to the presence of seawater-derived fluids or the oxidation of Fe^{2+} during serpentinization (Niu, 2004). However, some researchers (Bodinier & Godard, 2003; Boschi et al., 2006a) suggest that the LREE enrichment observed in ophiolitic and oceanic harzburgites may result from the infiltration of small volumes of evolved, LREE-enriched melts that precipitate minute amounts of barely detectable LREE-rich mineral phases. Because the in situ REE analyses of the serpentine minerals in the N. Apennine sequences show strong LREE depletions, we infer that a small-scale, “cryptic” melt impregnation may have occurred before serpentinization began, and any LREE-enriched phase that contributes to the LREE-enriched bulk rock pattern was not measured by the in situ analyses of the major mineral phases.

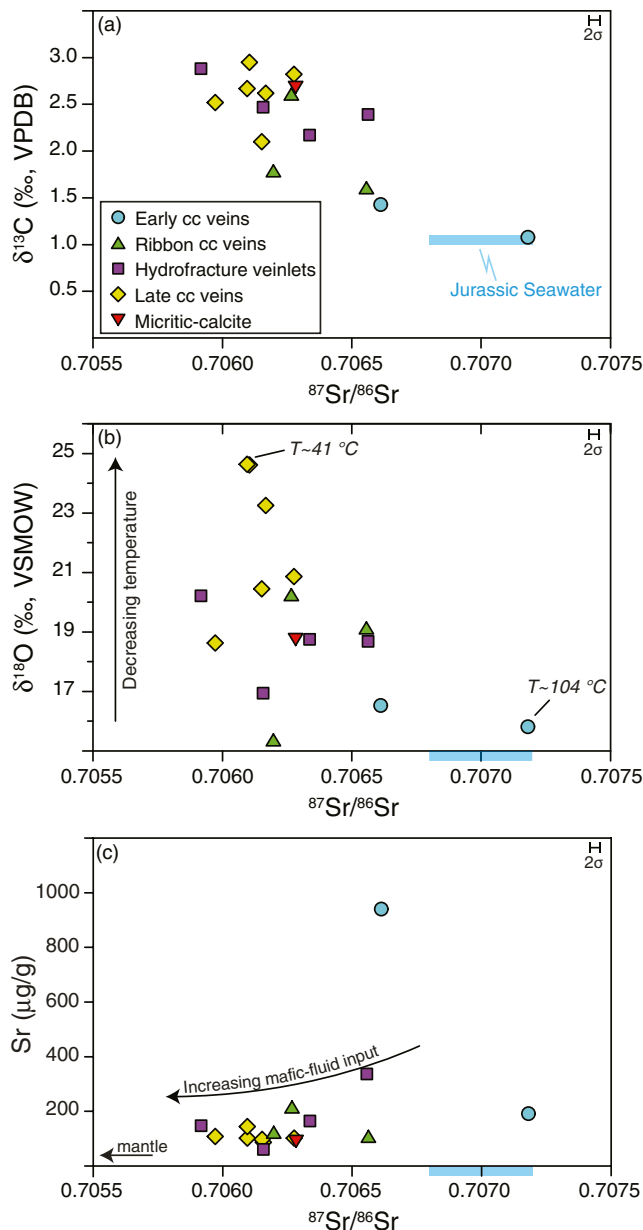


Figure 9. (a) Carbon ($\delta^{13}\text{C}_{\text{carb}}$) and (b) oxygen ($\delta^{18}\text{O}_{\text{carb}}$) isotope compositions, and (c) Sr concentrations vs. $^{87}\text{Sr}/^{86}\text{Sr}$ ratios of calcite veins and micritic carbonate. $\delta^{18}\text{O}$ values reflect decreasing temperatures with increasing input of mafic-derived fluid. Jurassic $^{87}\text{Sr}/^{86}\text{Sr}$ seawater composition as in Figure 8 and assuming $\delta^{13}\text{C} \approx 1\text{‰}$ after Veizer et al. (1999).

5.3. Fluid Sources During Serpentinization and Carbonation

Seawater is the primary fluid source in peridotite-hosted hydrothermal systems, as is reflected by seawater-like $^{87}\text{Sr}/^{86}\text{Sr}$ values found in serpentinites and their carbonate veins, such as from the Atlantic Ocean (e.g., Delacour et al., 2008; Vils et al., 2009). In the N. Apennine ophiolite, geochemical evidence for seawater-infiltration is documented in the carbon isotope compositions (see also Schwarzenbach, Früh-Green, Bernasconi, Alt, & Plas, 2013) and the $^{87}\text{Sr}/^{86}\text{Sr}$ values of some micro-drilled carbonate veins (Figure 9a). The early calcite veins have $^{87}\text{Sr}/^{86}\text{Sr}$ ratios of 0.70661–0.70718 and $\delta^{13}\text{C}$ values around 1‰, both reflecting average mid- to late Jurassic seawater compositions ($^{87}\text{Sr}/^{86}\text{Sr} \approx 0.7068\text{--}0.7070$, $\delta^{13}\text{C} \approx 1\text{‰}$, respectively) (Veizer et al., 1999; Wierzbowski et al., 2017). The effects of seawater infiltration within the serpentinites and ophiolites are further documented by the enrichment of FMEs with distinct positive anomalies in Cs, U, and Sr (Figure 7a). These enrichments are typical for seafloor-exposed serpentinites (Deschamps et al., 2012; Peters et al., 2017) and indicate infiltration of seawater-derived fluids during the main stages of serpentinization. The N. Apennine ophiolites show stronger enrichments in Cs, Sr, and Rb (and variable enrichments in U) (see Figure S1) suggesting overall higher fluid-rock ratios during formation of the ophiolites compared to the serpentinites.

Oxygen and hydrogen isotope compositions provide further constraints on fluid sources, water-rock ratios, and temperatures during water-rock interaction (e.g., Früh-Green et al., 1996; Sakai et al., 1990). Previous studies have suggested that fluid-rock interaction in the N. Apennine serpentinites took place at $\sim 150\text{--}240^\circ\text{C}$ based on bulk rock $\delta^{18}\text{O}$ values of 6.7–9.9‰ and assuming interaction with Jurassic seawater (Schwarzenbach, Früh-Green, Bernasconi, Alt, & Plas, 2013). The $\delta^{18}\text{O}_{\text{WR}}$ values of the samples studied here are within a slightly larger range (5.1–14.8‰; Table 1), but overall suggest a similar temperature range of 180°C – 280°C depending on which fractionation factor is used (see Figure S2). Comparison to available δD and $\delta^{18}\text{O}$ data from mid-ocean ridge serpentinites shows considerable overlap (Figure 10a). The range in $\delta^{18}\text{O}$ data mostly reflects variable serpentinization temperatures and variable water-rock ratios, with $\delta^{18}\text{O}$ values $>5.5\text{‰}$ (i.e., mantle values) generally suggesting temperature $<250^\circ\text{C}$ and $\delta^{18}\text{O}$ values $<5.5\text{‰}$ indicating higher temperatures (e.g., Alt, Shanks, et al., 2007; Barnes, Paulick, et al., 2009; Boschi, Bonatti, et al., 2013; Früh-Green et al., 1996; Sakai et al., 1990; Wenner & Taylor, 1973). In addition, the range in δD values of -86 to -59‰ determined in our study provide further evidence that most serpentinites studied to date have strongly negative δD values (Figure 10a). The origin of these negative δD values is still controversial. A common interpretation is that they require interaction with either evolved seawater-derived and/or magmatic waters, which are characterized by negative δD values (Früh-Green et al., 1996; Shanks et al., 1995; Wenner & Taylor, 1973). Alternatively, Früh-Green et al. (1996) proposed that the negative δD

values are correlated to the formation of considerable amounts of H_2 due to oxidation of ferrous iron in olivine \pm pyroxene. Finally, negative δD values in ophiolites potentially also derive from interaction with meteoric waters, which could have interacted with the serpentinites subsequent to their emplacement on the continent. This has previously been inferred based on highly variable δD values that correlated with mineral textures (Kyser et al., 1999). In this case, the δD values are lowered to more negative values commonly reaching δD values of -100‰ and lower (Barnes, Selverstone, & Sharp, 2006; Kyser et al., 1999). In the N. Apennine samples, the δD values have a relatively narrow range, which overlaps considerably with

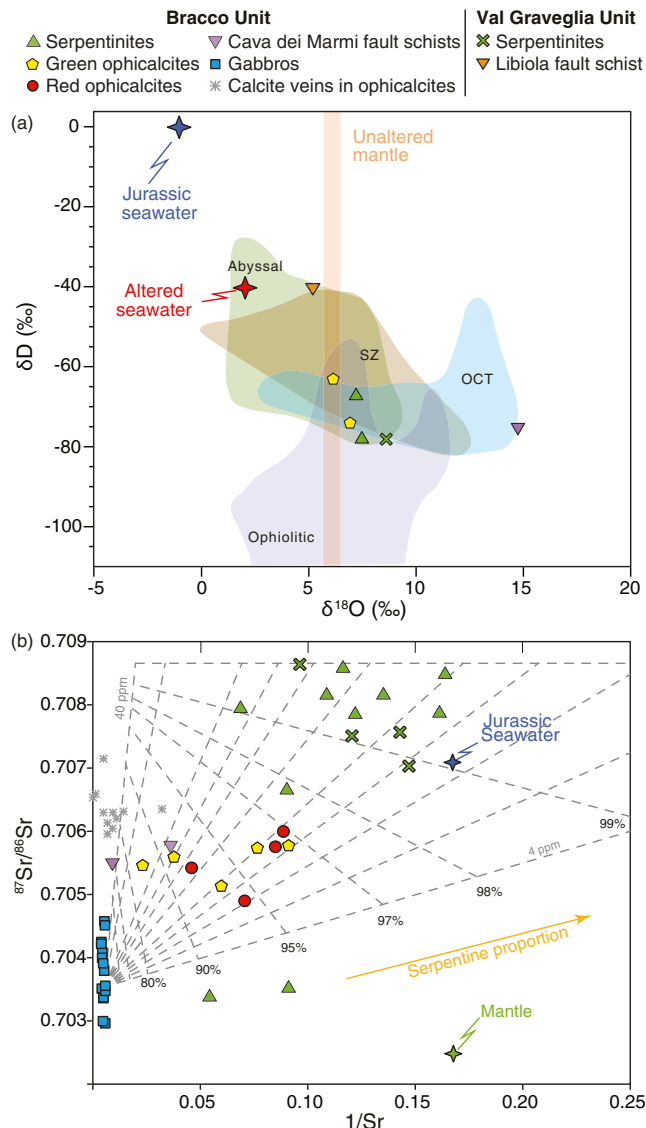


Figure 10. Geochemical models of interacting fluids. (a) $\delta^{18}\text{O}$ vs. δD plot of the serpentinite bulk rock compositions. Isotope ranges for unaltered mantle ($5.8 \pm 0.3\text{‰}$) and abyssal, ocean-continent transition zones (OCT), subduction zone and arc settings (SZ), and ophiolitic serpentinites (including subducted ophiolites) from Agrinier and Girardeau (1988), Barnes, Eldam, et al. (2013), Barnes, Paulick, et al. (2009), Boschi, Bonatti, et al. (2013), Fröh-Green et al. (1996), Sakai et al. (1990), Wenner and Taylor (1973, 1974). (b) $^{87}\text{Sr}/^{86}\text{Sr}$ vs. $1/\text{Sr}$ for bulk rock samples. Dotted gray lines represent simple fluid-rock interaction trajectories, indicating mixing between a serpentinite end-member and a gabbro-derived fluid, formed by altered seawater and assumed to have similar compositions as the analyzed gabbros. Percentages indicate mixing proportions between gabbro and serpentine. Opicalcites plot within the mixing trends, suggesting mafic-derived fluids affected the opicalcites. Serpentinites display higher $^{87}\text{Sr}/^{86}\text{Sr}$ compositions than Jurassic seawater, suggesting the influence of fluids with more radiogenic Sr. Jurassic seawater and mantle as in Figure 8.

the δD and $\delta^{18}\text{O}$ values seen in abyssal serpentinites and serpentinites in OCT settings (Agrinier & Girardeau, 1988; Barnes, Paulick, et al., 2009; Boschi, Bonatti, et al., 2013; Fröh-Green et al., 1996) (Figure 10a). In addition, we find no evidence for past or current interaction by meteoric waters (as e.g., seen in the Oman ophiolite (Kelemen et al., 2020)), nor do we find mineralogical evidence for serpentine recrystallization or surface weathering that would indicate either interaction with meteoric fluids or the effect of low-grade metamorphic overprint. Sample recovery from quarries also allowed for fresh sample material to be collected. Thus, we argue that the measured δD values are most likely the result of seafloor processes and that interaction with an evolved seawater-derived fluid possibly with a magmatic component resulted in the negative δD values and affected both bulk serpentinites and opicalcites in about equal proportions (Fröh-Green et al., 1996; Shanks et al., 1995).

5.4. Silica Metasomatism

The abundance of talc (macroscopically seen in Figures 2b and 3) and amphibole in the opicalcites as well as serpentine-talc intergrowths in the serpentinite mesh textures (Figure 4) document an increase in SiO_2 bulk content from the basement serpentinites to the opicalcites, and suggests localized Si-metasomatism. Si-metasomatism in the opicalcites is also expressed by lower MgO/SiO_2 ratios (Figure 6) compared to the basement serpentinites, as is seen in a plot of MgO/SiO_2 vs. $\text{Al}_2\text{O}_3/\text{SiO}_2$ (Figure 11), where the terrestrial array is defined by the successive magmatic depletion of a primitive mantle during partial melting (Hart & Zindler, 1986; Jagoutz et al., 1979). An off-set to lower MgO/SiO_2 values in most abyssal serpentinites has previously been related to partial MgO loss during seafloor weathering through brucite dissolution and incongruent olivine dissolution (Niu, 2004; Paulick et al., 2006; Snow & Dick, 1995). However, the macroscopic abundance of talc in the Bracco opicalcites leads us to infer that the lower MgO/SiO_2 ratios are more likely the result of Si addition rather than extensive Mg loss (Malvoisin, 2015).

Si-metasomatism and/or talc formation have previously been documented in peridotites from the MAR, including ODP Leg 209 near the $15^\circ 20'\text{N}$ fracture zone (Paulick et al., 2006) and the AM (Boschi et al., 2006a, 2006b). In both cases, alteration is associated with the input of fluids derived from peridotite or gabbro alteration at depth, which resulted either in pervasive talc alteration in the peridotites (Paulick et al., 2006) or by localized influx of oxidizing, Si-Al-Ca-rich fluids produced talc, amphibole, and chlorite schists along fault zones (e.g., at the AM; Boschi et al., 2006a; Boschi et al., 2006b). Accordingly, we suggest that in the rocks studied here, Si-metasomatism could have been caused by two possible mechanisms: 1) seawater mixing with fluids generated from the serpentinization of peridotites, specifically pyroxenes, at increasing water-rock ratios or 2) interaction with fluids with a component derived from a mafic source. Both processes have been thermodynamically modeled by Malvoisin (2015) and resulted in formation of talc coexisting with either serpentine or carbonate. Considering the amount of talc precipitated as druses in the opicalcites and the shift to higher SiO_2 bulk rock contents in most opicalcites, we tend toward an externally derived fluid to account for the late stage Si-metasomatism.

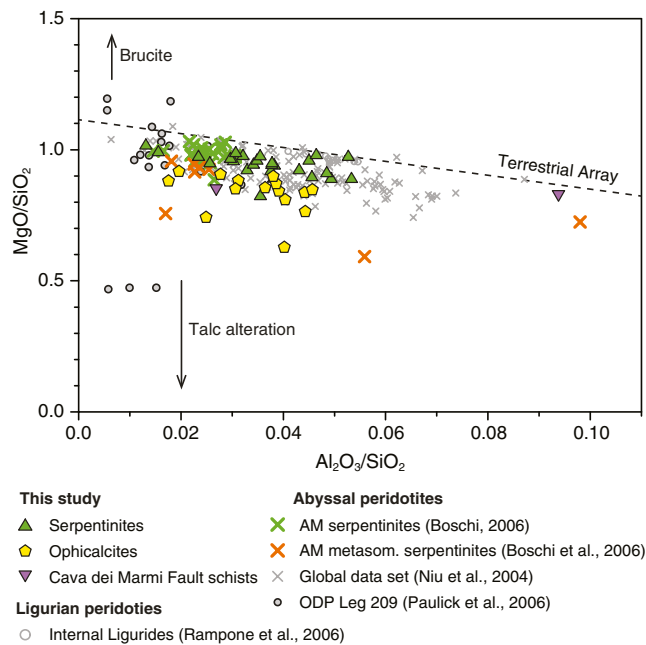


Figure 11. Plot of MgO/SiO_2 vs. $\text{Al}_2\text{O}_3/\text{SiO}_2$ comparing the Bracco Unit with other Ligurian peridotites and abyssal peridotites. “Terrestrial Array” represents unaltered peridotite compositions after Jagoutz et al. (1979).

Higher enrichments in Sr, Rb, and Cs in the ophicalcites provide further evidence for a mafic source of the fluid, such as gabbroic intrusions or basaltic lavas (von Damm, 1990) (Figure 7a). Interestingly, Ba, which is considered to be highly mobile in high-temperature fluids and can be enriched in fluids derived from young gabbroic intrusions, is not markedly enriched. In addition, there is a lack of metal enrichments (e.g., Cu or Zn), which is also typical for high-temperature fluid-rock interaction (e.g., Niu, 2004; von Damm, 1990). This would suggest that the fluids that produced the Si-metasomatism in the ophicalcites were dominantly lower temperature fluids and hence, would not have affected Ba and metal concentrations. Additional evidence for mafic-derived fluids is provided by the Sr isotope signatures. The final formation of talc filling druses within pre-existing carbonate veins in the ophicalcites (Figure 3) correlates with an increase in the $^{87}\text{Sr}/^{86}\text{Sr}$ ratios from seawater-like compositions in the early calcite veins toward mantle or MORB-like $^{87}\text{Sr}/^{86}\text{Sr}$ ratios in the later stage carbonate veins (Figure 9c). In addition, we calculated simple isotope mixing trajectories between serpentinites and mafic-derived end-member fluids (Figure 10b). For this we used different Sr concentrations for the serpentine (4–15 $\mu\text{g/g}$), the highest serpentinite compositions ($^{87}\text{Sr}/^{86}\text{Sr} = 0.7085$) and the average of the analyzed gabbroic rocks ($^{87}\text{Sr}/^{86}\text{Sr} = 0.7037$), which is assumed to approximate the composition of the mafic-derived fluids. All the ophicalcites and Cava dei Marmi fault schists indicate variable proportions of mixing between the two end-members. Similarly, most late calcite veins have $^{87}\text{Sr}/^{86}\text{Sr}$ ratios between those of Jurassic seawater and the gabbros (Figures 9 and 10b).

We infer that the trend to lower $^{87}\text{Sr}/^{86}\text{Sr}$ ratios reflect increasing influx of mafic-derived fluids with ongoing rock fracturing associated with more pronounced Si-influx in the ophicalcites than the underlying serpentinites. Associated $\delta^{13}\text{C}$ -values of 2–3‰ overlap with values from carbonate vent samples, breccias, and carbonate infillings from the LCHF and are attributed to the input of ^{13}C -enriched carbon associated with ongoing microbial activity (e.g., methanogenesis) (Früh-Green et al., 2003). An abundance of methanogenesis agrees with the decreasing temperatures preserved in the $\delta^{18}\text{O}_{\text{carb}}$ values (Figure 9b), which increasingly favors microbial activity. Alternatively, they may be the result of closed system fluid evolution of the dissolved inorganic carbon during water-rock interaction with the mafic lithologies.

The Cava dei Marmi fault schist that displays a high $\delta^{18}\text{O}_{\text{serp}}$ value yielded low $^{87}\text{Sr}/^{86}\text{Sr}$ ratios (Figure 10b), which are in the same range as the ophicalcites, suggesting that these fault schists and the ophicalcites were altered by the same or compositionally similar fluids. In contrast, the Libiola fault schist is characterized by elevated $^{87}\text{Sr}/^{86}\text{Sr}$ ratios (up to 0.71847), and based on the oxygen composition, has the highest formation temperatures (lowest $\delta^{18}\text{O}$ value). Such compositions may imply that a sedimentary influx took effect during hydrothermal alteration on the ocean floor or that the schists may have been reactivated during Alpine orogenesis.

5.5. Evidence for Fluid Input From Continental Basement Rocks

Interestingly, most of the serpentinites have higher $^{87}\text{Sr}/^{86}\text{Sr}$ values than Jurassic seawater (Figure 8), which varied between 0.7068 and 0.7072 in the Middle to Late Jurassic (Wierzbowski et al., 2017), whereas $^{87}\text{Sr}/^{86}\text{Sr}$ values above 0.7078 were only reached at ~74 Ma (Jones et al., 1994). $^{87}\text{Sr}/^{86}\text{Sr}$ values above seawater compositions have also been documented in some serpentinites from the MAR (e.g., Mével, 2003; Snow et al., 1993) suggesting a ^{87}Sr reservoir during hydrothermal circulation. Snow et al. (1993) argue that high $^{87}\text{Sr}/^{86}\text{Sr}$ ratios could be generated by infiltration of detrital sediments penetrated through micro-cracks into serpentinites. This process is not directly related to serpentinization but can considerably alter the $^{87}\text{Sr}/^{86}\text{Sr}$ compositions of abyssal serpentinites (Mével, 2003). Thus, one possibility would be that interaction of fluids with the sedimentary Framura Breccia overlying the ophicalcites could have had an effect on the serpentinites. However, the ophicalcites, which are underlying the sedimentary Framura Breccia and overlying the

serpentinites, do not show this more radiogenic Sr enrichment. Alternatively, continental basement rocks have high $^{87}\text{Sr}/^{86}\text{Sr}$ ratios (>0.720 to 0.750 ; Allègre, 2008) similar to sedimentary rocks and, thus, fluids that interacted with continental basement could have modified the $^{87}\text{Sr}/^{86}\text{Sr}$ ratios of the serpentinites. Recent models suggest that continental basement was likely present during initial stages of rifting and opening of the Piemonte-Ligurian ocean, where subcontinental mantle was sporadically exposed to seawater in a narrow ocean basin (Le Breton et al., 2021). Similarly, felsic continental crust associated with subcontinental mantle in the N. Apennines have been interpreted as evidence for the early stages of continental breakup and opening of the oceanic basement within an OCT (Marroni et al., 1998) and have been compared to observations from the Iberia-Newfoundland margins where tilted continental basement blocks and oceanic crust periodically occur over a distance of 150 km within the OCT (McCarthy et al., 2018; Whitmarsh et al., 2001). Such a setting would allow infiltration of fluids that had interacted with continental basement rocks during initial stages of peridotite hydration, shifting the $^{87}\text{Sr}/^{86}\text{Sr}$ ratios of the serpentinites to higher values. This interpretation, however, assumes that the early continental Sr isotope signatures are preserved throughout the hydrothermal evolution of the system. Alternatively, we would have to envisage exchange with continental rocks and preferential fluid circulation solely in the serpentinites during the Alpine orogeny, for which we have no further evidence.

6. Hydrothermal Evolution of the Northern Apennine Ophiolite

The data presented above suggest a complex alteration history and indicate that the serpentinites were dominated by different fluids than the overlying ophicalcites, but all record multiple phases of water-rock interaction, some of which result in pervasive alteration whereas other events were more localized (e.g., forming distinct veins). Using our new data with previously published interpretations, we reconstruct the temporal and chemical evolution of the studied rocks and infer the alteration history of the N. Apennine ophiolite sequence.

The formation of tremolite to hornblende rims around pyroxene suggests that the peridotites of the N. Apennine were initially hydrated at relatively high temperatures likely during initial mantle upwelling. These stages of mantle hydration as well as continuous mantle exhumation were affected by fluids that had reacted with either the continental basement or with sediments prior to peridotite infiltration (Figure 12—stage 1). Since continental basement rocks and sedimentary sequences have considerably more radiogenic Sr compared to peridotites, even low amounts of fluid that had interacted with basement rocks or sediments would have substantially shifted the $^{87}\text{Sr}/^{86}\text{Sr}$ values of the serpentinized peridotites to higher values. The serpentinites from the Bracco and the Val Graveglia Units both show the same trends further supporting wide-spread and relatively pervasive fluid infiltration with a more radiogenic Sr signature. Seawater influx was overall relatively restricted as suggested by the lesser enrichment of FMEs such as Cs, Rb, Sr, U in the serpentinites compared to the ophicalcites. Based on the flat REE patterns of the peridotites cryptic melt impregnation likely also affected these rocks.

Serpentinization was also associated with the local influx of higher temperature fluids. This is documented by the formation of edenite and Mg-hornblende, indicating amphibolite-facies conditions, that form veins together with chlorite or replace bastites. In addition, high-temperature fluid influx is recorded by sulfur isotope signatures. Using in situ $\delta^{34}\text{S}$ values in sulfide minerals and bulk rock multiple sulfur isotope signatures, Schwarzenbach, Gill, and Johnston (2018) document the impact of thermochemical sulfate reduction, which took place at $\sim 350^\circ\text{C}$ – 400°C and was associated with input of H_2S leached from mafic rocks. This stage of alteration likely took place during continuous uplift of the peridotites during the main stage of serpentinization as some of the amphibole-chlorite-veins cut the serpentine mesh texture. Gabbroic intrusions most likely provided the heat for high-T fluid circulation (Figure 12—stage 2). At a similar time, the Cava dei Marini fault schists likely formed within fault zones during peridotite exposure, similar to the processes described at the AM (e.g., Boschi et al., 2006a; Früh-Green et al., 2018; Rouméjon et al., 2018).

By continuous uplift of the peridotites, these rocks were exhumed to the seafloor where serpentinization fluids mixed with seawater in cracks and fractures producing carbonate veins in the serpentinites and ophicalcites (Figure 12—stage 3). These veins document temperatures decreasing from 150°C to 41°C with increasing seawater influx (this study and Schwarzenbach, Früh-Green, Bernasconi, Alt, & Plas, 2013). As

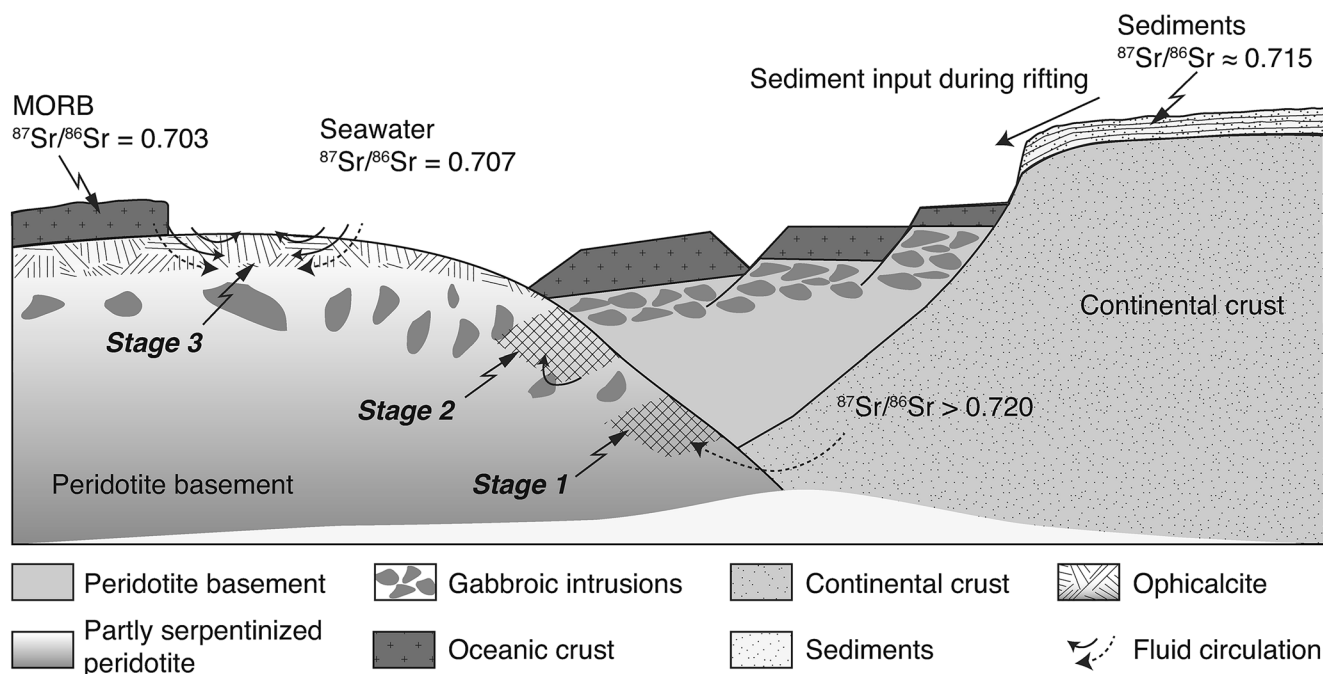


Figure 12. Schematic representation of the hydrothermal evolution of the N. Apennine serpentinites and opihalcites (tectonic model adapted from Manatschal & Müntener, 2009). Stage 1: initial stages of serpentinization by fluids with radiogenic Sr e.g., from continental basement rocks or sediments. Stage 2: continuous uplift and serpentinization with local influx of high temperature fluids (derived from gabbroic intrusions) producing rare talc, chlorite, and amphibole with hornblende to edenite compositions as veins or replacing pyroxene. Stage 3: final stages of alteration and exposure to seawater documented by carbonate veins with seawater-like Sr isotope compositions. Subsequent extrusion of basaltic lavas on top of the opihalcites and continuous water-rock interaction led to Si metasomatism (with SiO₂ provided by the lavas) and talc formation predominantly in the opihalcites. See text for discussion.

the system cooled, microbial activity took place as documented by sulfur isotope compositions in sulfide minerals (Schwarzenbach, Gill, & Johnston, 2018) and the $\delta^{13}\text{C}$ values of the carbonates that point to methanogenesis. At this stage the highly oxidized opihalcites would have been directly exposed to seawater. Extensive and pervasive interaction with seawater in the opihalcites is indicated by greater enrichments in FMEs (Cs, Rb, Sr, and locally U) compared to the serpentinites. However, some of this enrichment may also be linked to later Si-metasomatism.

Interestingly, most of the Sr values of the calcite veins in the opihalcites are significantly below Jurassic seawater and only a few of the veins reflect unmodified seawater based on their $^{87}\text{Sr}/^{86}\text{Sr}$ ratios. As discussed above, these low $^{87}\text{Sr}/^{86}\text{Sr}$ ratios can be correlated with the Si-metasomatism recorded in the opihalcites and are likely produced by Si input from mafic rocks. However, the serpentinites underlying the opihalcites have significantly higher $^{87}\text{Sr}/^{86}\text{Sr}$ ratios than the opihalcites suggesting that the Si-metasomatism was most pronounced in the top most sections and decreased downwards, consistent with the presence of talc filling late stage carbonate veins. Underlying gabbro intrusions are therefore unlikely the fluid source. The most likely scenario is that the fluids leading to Si-metasomatism were derived from interaction with basalts, which are locally found overlying the opihalcites (B. E. Treves and Harper, 1994). Consequently, we infer that seawater-derived fluids infiltrated the basalts after their emplacement, picked up the $^{87}\text{Sr}/^{86}\text{Sr}$ signal of the basalts and then infiltrated the opihalcites to produce talc in druses within preexisting carbonate veins. As the fluids would have come from the top, restricted fluid infiltration associated with Si-metasomatism would not have affected the underlying serpentinites. In addition, it should be noted that the serpentinite protolith of the opihalcites would initially have had an $^{87}\text{Sr}/^{86}\text{Sr}$ ratio above Jurassic seawater and would have later entirely shifted (during their conversion from serpentinites to opihalcites) toward basalt-like $^{87}\text{Sr}/^{86}\text{Sr}$ values. This shift would have accompanied extensive alteration and precipitation of talc in druses. Finally, the bulk rock δD and $\delta^{18}\text{O}$ values record the integrated history of fluid infiltration, which was overall dominated by evolved, seawater-derived fluids, but that possibly contained a magmatic fluid component.

7. Conclusions

This study summarizes the extensive alteration history of opicalcites and serpentinites in the N. Apennine ophiolite. The mineralogical and geochemical signatures of the serpentinites and opicalcites record extensive metasomatism by fluids with variable chemical compositions and a cryptic melt impregnation pre-dating hydrothermal alteration. In particular, the chemical variations attest to fluids of variable origin, i.e., seawater-derived fluids that have interacted with different lithologies and imprint a chemical signature on the ultramafic basement as it is undergoing hydration. The serpentinites thereby record 1) hydration processes during early mantle upwelling within an opening ocean basin with input of a continental basement-derived fluid—as preserved in the high $^{87}\text{Sr}/^{86}\text{Sr}$ ratios; and 2) localized high-temperature fluid influx likely associated with continuous mantle exposure and local gabbroic intrusion as documented by amphiboles with hornblende to edenite composition and sulfide isotope compositions as previously reported. In contrast, the opicalcites mostly record the late stages of seawater-rock interaction with extensive carbonation and interaction with basalt-derived fluids at low-temperatures as the mantle sequence was emplaced at the ocean floor, resulting in a gain of SiO_2 , CaO , and FMEs. Although all studied rocks record multiple phases of water-rock interaction, their chemical signatures are dominated by different and distinct events. Accordingly, the transition from serpentinite to opicalcite as preserved in the N. Apennine ophiolite records the history of uplift and exposure on the seafloor. In addition, this alteration sequence documents that serpentinites can undergo a very complex hydrothermal evolution from serpentinization, carbonation to Si-metasomatism. The complex hydrothermal evolution of these systems is essential to understand the chemical and petrophysical evolution of the oceanic lithosphere and processes of mass transfer. Extensive carbonation and Si-metasomatism may eventually affect subduction zone processes, i.e., change the expected rheology, for example, due to higher Si contents, and mineral stabilities within the subducting slab and the subduction zone channel, and as a consequence may affect element cycling within subduction zones.

Data Availability Statement

All data sets for this research are included in this paper and its supplementary information files Tables S1–S5. In addition, all supplementary data is available online on PANGAEA at <https://doi.org/10.1594/PANGAEA.921751>.

Acknowledgments

We thank Giancarlo Molli for help during fieldwork and for offering the gabbro samples for this study. We also thank Peter Ulmer and Derek Vance for their contribution to the interpretation of the data. We are grateful to Corey Archer, Giuditta Fellin, Ilaria Baneschi, Benita Putlitz, Ruth Hindshaw, and Gregory de Souza for their valuable help during the analytical procedures. This work was supported by Swiss SNF Grants 200021-134947 and 200020-146886 to Früh-Green. This contribution benefited greatly from the constructive comments by the associate editor, and extensive reviews by Benjamin Malvoisin and an anonymous reviewer, whom we gratefully thank. Open Access enabled and organized by Projekt DEAL.

References

- Agrinier, P., & Girardeau, J. (1988). Hydrothermal alteration of the peridotites cored at the ocean/continent boundary of the Iberian Margin: Petrologic and stable isotope evidence. *Proceedings of the ocean drilling program, scientific results*, Vol. 103, 225–234.
- Allègre, C. J. (2008). *Isotope geology*. New York: Cambridge University Press. <https://doi.org/10.1017/cbo9780511809323>
- Alt, J. C., Crispini, L., Gaggero, L., Levine, D., Lavagnino, G., Shanks, W. C., & Gulbransen, C. (2018). Normal faulting and evolution of fluid discharge in a Jurassic seafloor ultramafic-hosted hydrothermal system. *Geology*, 2018. <https://doi.org/10.1130/G40287.1>
- Alt, J. C., Schwarzenbach, E. M., Früh-Green, G. L., Shanks, W. C., III, Bernasconi, S. M., Garrido, C. J., et al. (2013). The role of serpentinites in cycling of carbon and sulfur: Seafloor serpentinization and subduction metamorphism. *Lithos*, 178, 40–54. <https://doi.org/10.1016/j.lithos.2012.12.006>
- Alt, J. C., Shanks, W. C., Bach, W., Paulick, H., Garrido, C. J., & Beaudoin, G. (2007). Hydrothermal alteration and microbial sulfate reduction in peridotite and gabbro exposed by detachment faulting at the Mid-Atlantic Ridge, 15° 20'N (ODP Leg 209): A sulfur and oxygen isotope study. *Geochemistry, Geophysics, Geosystems*, 8. <https://doi.org/10.1029/2007gc001617>
- Bach, W., Garrido, C. J., Paulick, H., Harvey, J., & Rosner, M. (2004). Seawater-peridotite interactions: First insights from ODP Leg 209, MAR 15°N. *Geochemistry, Geophysics, Geosystems*, 5(22). <https://doi.org/10.1029/2004gc000744>
- Barnes, J. D., Eldam, R., Lee, C.-T. A., Errico, J. C., Loewy, S., & Cisneros, M. (2013). Petrogenesis of serpentinites from the Franciscan complex, western California, USA. *Lithos*, 178(0), 143–157. <https://doi.org/10.1016/j.lithos.2012.12.018>
- Barnes, J. D., Paulick, H., Sharp, Z. D., Bach, W., & Beaudoin, G. (2009). Stable isotope ($\delta^{18}\text{O}$, δD , $\delta^{37}\text{Cl}$) evidence for multiple fluid histories in mid-Atlantic abyssal peridotites (ODP Leg 209). *Lithos*, 110, 83–94. <https://doi.org/10.1016/j.lithos.2008.12.004>
- Barnes, J. D., Selverstone, J., & Sharp, Z. D. (2006). Chlorine isotope chemistry of serpentinites from Elba, Italy, as an indicator of fluid source and subsequent tectonic history. *Geochemistry, Geophysics, Geosystems*, 7. <https://doi.org/10.1029/2006gc001296>
- Beard, J. S., Frost, B. R., Fryer, P., McCaig, A., Searle, R., Ildefonse, B., et al. (2009). Onset and progression of serpentinization and magnetite formation in olivine-rich troctolite from IODP Hole U1309D. *Journal of Petrology*, 50, 387–403. <https://doi.org/10.1093/petrology/egp004>
- Bodinier, J.-L., & Godard, M. (2003). Orogenic, ophiolitic, and abyssal peridotites. In H. D. & K. K. Turekian (Eds.), *Treatise on geochemistry*, Holland. Elsevier Ltd.
- Boschi, C., Bonatti, E., Ligi, M., Brunelli, D., Cipriani, A., Dallai, L., et al. (2013). Serpentinization of mantle peridotites along an uplifted lithospheric section, Mid-Atlantic Ridge at 11°N. *Lithos*, 178, 3–23. <https://doi.org/10.1016/j.lithos.2013.06.003>
- Boschi, C., Dini, A., Baneschi, I., Bedini, F., Perchiazzi, N., & Cavallo, A. (2017). Brucite-driven CO_2 uptake in serpentinized dunites (Ligurian Ophiolites, Montecastelli, Tuscany). *Lithos*, 288–289, 264–281. <https://doi.org/10.1016/j.lithos.2017.07.005>

- Boschi, C., Dini, A., Früh-Green, G. L., & Kelley, D. S. (2008). Isotopic and element exchange during serpentinization and metasomatism at the Atlantis Massif (MAR 30°N): Insights from B and Sr isotope data. *Geochimica et Cosmochimica Acta*, 72, 1801–1823. <https://doi.org/10.1016/j.gca.2008.01.013>
- Boschi, C., Früh-Green, G. L., Delacour, A., Karson, J. A., & Kelley, D. S. (2006a). Mass transfer and fluid flow during detachment faulting and development of an oceanic core complex, Atlantis Massif (MAR 30°). *Geochemistry, Geophysics, Geosystems*, 7. <https://doi.org/10.1029/2005gc001074>
- Boschi, C., Früh-Green, G. L., & Escartin, J. (2006b). Occurrence and significance of serpentinite-hosted, talc- and amphibole-rich fault rocks in modern oceanic settings and ophiolite complexes: An overview. *Ophioliti*, 31, 129–140.
- Brazelton, W. J., Schrenk, M. O., Kelley, D. S., & Baross, J. A. (2006). Methane- and sulfur-metabolizing microbial communities dominate the lost city hydrothermal field ecosystem. *Applied and Environmental Microbiology*, 72, 6257–6270. <https://doi.org/10.1128/aem.00574-06>
- Breitenbach, S. F. M., & Bernasconi, S. M. (2011). Carbon and oxygen isotope analysis of small carbonate samples (20–100 µg) with a Gas-Bench II preparation device. *Rapid Communications in Mass Spectrometry*, 25, 1910–1914. <https://doi.org/10.1002/rcm.5052>
- Cannat, M., Fontaine, F., & Escartin, J. (2010). Serpentinization and associated hydrogen and methane fluxes at slow spreading ridges. In P. A. Rona, C. W. Devey, J. Dymant, & B. J. Murton (Eds.), *Diversity of hydrothermal systems on slow spreading ocean ridges. Geophysical monograph*. Washington: American Geophysical Union.
- Cannat, M., Mevel, C., Maia, M., Deplus, C., Durand, C., Gente, P., et al. (1995). *Thin crust, ultramafic exposures, and rugged faulting patterns at the Mid-Atlantic Ridge (22°N–24°N)*. *Geology*, 23, 49–52. [https://doi.org/10.1130/0091-7613\(1995\)023<0049:tcuear>2.3.co;2](https://doi.org/10.1130/0091-7613(1995)023<0049:tcuear>2.3.co;2)
- Cannat, M., Sauter, D., Mendel, V., Ruellan, E., Okino, K., Escartin, J., et al. (2006). *Modes of seafloor generation at a melt-poor ultraslow-spreading ridge*. *Geology*, 34, 605–608. <https://doi.org/10.1130/g22486.1>
- Cogné, J.-P., & Humler, E. (2006). Trends and rhythms in global seafloor generation rate. *Geochemistry, Geophysics, Geosystems*, 7. <https://doi.org/10.1029/2005gc001148>
- Coleman, R. G. (1977). *Ophiolites*. New York: Springer-Verlag. <https://doi.org/10.1007/978-3-642-66673-5>
- Cortesogno, L. (1981). *Carta geologica delle ophioliti del Bracco tra Lèvanto e Velva*. Firenze, S.E.L.C.A.
- Cortesogno, L., Galbiati, B., & Principi, G. (1980). Le breccie serpentinitiche giurassiche della Liguria orientale. In *Symposium "On tectonic inclusions and associated rocks in serpentinites"* (Vol. 33, pp. 185–200). Geneva: Archive. Sc. Geneva.
- Cortesogno, L., Gianelli, G., & Piccardo, G. (1975). Preorogenic metamorphic and tectonic evolution of the ophiolite mafic rocks (Northern Apennine and Tuscany). *Italian Journal of Geosciences*, 94, 291–327.
- Delacour, A., Früh-Green, G. L., Frank, M., Gutjahr, M., & Kelley, D. S. (2008). Sr- and Nd-isotope geochemistry of the Atlantis Massif (30°N, MAR): Implications for fluid fluxes and lithospheric heterogeneity. *Chemical Geology*, 254, 19–35. <https://doi.org/10.1016/j.chemgeo.2008.05.018>
- Deniel, C., & Pin, C. (2001). Single-stage method for the simultaneous isolation of lead and strontium from silicate samples for isotopic measurements. *Analytica Chimica Acta*, 426, 95–103. [https://doi.org/10.1016/S0003-2670\(00\)01185-5](https://doi.org/10.1016/S0003-2670(00)01185-5)
- Deschamps, F., Godard, M., Guillot, S., Chauvel, C., Andreani, M., Hattori, K., et al. (2012). Behavior of fluid-mobile elements in serpentinites from abyssal to subduction environments: Examples from Cuba and Dominican Republic. *Chemical Geology*, 312–313, 93–117. <https://doi.org/10.1016/j.chemgeo.2012.04.009>
- de Souza, G. F., Reynolds, B. C., Kiczka, M., & Bourdon, B. (2010). Evidence for mass-dependent isotopic fractionation of strontium in a glaciated granitic watershed. *Geochimica et Cosmochimica Acta*, 74, 2596–2614. <https://doi.org/10.1016/j.gca.2010.02.012>
- Escartin, J., Hirth, G., & Evans, B. (1997). Effects of serpentinization on the lithospheric strength and the style of normal faulting at slow spreading ridges. *Earth and Planetary Science Letters*, 151, 181–189. [https://doi.org/10.1016/S0012-821X\(97\)81847-X](https://doi.org/10.1016/S0012-821X(97)81847-X)
- Friedman, I., & O'Neil, J. R. (1977). Compilation of stable isotope fractionation factors of geochemical interest. In *Data of geochemistry*. U.S. Geological Survey. <https://doi.org/10.3133/pp440kk>
- Früh-Green, G. L., Connolly, J. A., Plas, A., Kelley, D. S., & Grobéty, B. (2004). Serpentinization of oceanic peridotites: Implications for geochemical cycles and biological activity. In *The seafloor biosphere at Mid-Ocean Ridges*. Washington D.C: American Geophysical Union.
- Früh-Green, G. L., Kelley, D. S., Bernasconi, S. M., Karson, J. A., Ludwig, K. A., Butterfield, D. A., et al. (2003). 30,000 yr of hydrothermal activity at the Lost City Vent field. *Science*, 301, 495–498. <https://doi.org/10.1126/science.1085582>
- Früh-Green, G. L., Orcutt, B. N., Rouméjon, S., Lilley, M. D., Morono, Y., Cotterill, C., et al. (2018). Magmatism, serpentinization and life: Insights through drilling the Atlantis Massif (IODP Expedition 357). *Lithos*, 323, 137–155. <https://doi.org/10.1016/j.lithos.2018.09.012>
- Früh-Green, G. L., Plas, A., & Lécuyer, C. (1996). Petrologic and stable isotope constraints on hydrothermal alteration and serpentinization of the EPR shallow mantle at Hess Deep (Site 895). *Proceedings of the ocean drilling program, scientific results*, Vol. 147, 255–291.
- Früh-Green, G. L., Weissert, H., & Bernoulli, D. (1990). A multiple fluid history recorded in Alpine ophiolites. *Journal of the Geological Society*, 147, 959–970. <https://doi.org/10.1144/gsjgs.147.6.0959>
- Garuti, G., Bartoli, O., Scacchetti, M., & Zaccarini, F. (2008). Geological setting and structural styles of volcanic massive sulfide deposits in the Northern Apennines (Italy): Evidence for seafloor and sub-seafloor hydrothermal activity in unconventional ophiolites of the Mesozoic Tethys. *Boletín de la Sociedad Geológica Mexicana*, 60, 121–145. <https://doi.org/10.18268/bsgm2008v60n1a9>
- Grozeva, N. G., Klein, F., Seewald, J. S., & Sylva, S. P. (2017). Experimental study of carbonate formation in oceanic peridotite. *Geochimica et Cosmochimica Acta*, 199, 264–286. <https://doi.org/10.1016/j.gca.2016.10.052>
- Guillong, M., Meier, D. L., Allan, M. M., Heinrich, C. A., & Yardley, B. (2008). A MATLAB-based program for the reduction of laser ablation ICP-MS data of homogeneous materials and inclusions. *Mineralogical Association of Canada Short Course*, 40, 328–333.
- Hart, S. R., & Zindler, A. (1986). In search of a bulk-Earth composition. *Chemical Geology*, 57, 247–267. [https://doi.org/10.1016/0009-2541\(86\)90053-7](https://doi.org/10.1016/0009-2541(86)90053-7)
- Jagoutz, E., Palme, H., Baddenhauser, H., Blum, K., Cendales, M., Dreibus, G., et al. (1979). The abundances of major, minor and trace elements in the Earth's mantle as derived from primitive ultramafic nodules. *Proceeding of Lunar Science Conference*, 10, 2031–2050.
- John, B. E., & Cheadle, M. J. (2010). Deformation and alteration associated with oceanic and continental detachment fault systems; Are they similar? In *Geochophysical monograph*.
- Jones, C. E., Jenkyns, H. C., Coe, A. L., & Stephen, H. P. (1994). Strontium isotopic variations in Jurassic and Cretaceous seawater. *Geochimica et Cosmochimica Acta*, 58, 3061–3074. [https://doi.org/10.1016/0016-7037\(94\)90179-1](https://doi.org/10.1016/0016-7037(94)90179-1)
- Karson, J. A., Früh-Green, G. L., Kelley, D. S., Williams, E. A., Yoerger, D. R., & Jakuba, M. (2006). Detachment shear zone of the Atlantis Massif core complex, Mid-Atlantic Ridge 30°N. *Geochemistry, Geophysics, Geosystems*, 7. <https://doi.org/10.1029/2005gc001109>
- Kelemen, P. B., Matter, J. M., Teagle, D. A. H., Coggon, J. A., & Team, a. t. O. D. P. S. (2020). Oman Drilling Project, Scientific Drilling in the Samail Ophiolite, Sultanate of Oman, International Ocean Discovery Program. <https://doi.org/10.14379/OmanDP.proc.2020>

- Kelley, D. S., Karson, J. A., Früh-Green, G. L., Yoerger, D. R., Shank, T. M., Butterfield, D. A., et al. (2005). A serpentinite-hosted ecosystem: The lost city hydrothermal field. *Science*, 307, 1428–1434. <https://doi.org/10.1126/science.1102556>
- Kelley, D. S., Karson, J. A., Karson, J. A., Blackman, D. K., Früh-Green, G. L., Butterfield, D. A., et al. (2001). An off-axis hydrothermal vent field near the Mid-Atlantic ridge at 30°N. *Nature*, 412, 145–149. <https://doi.org/10.1038/35084000>
- Klein, F., Bach, W., Humphris, S. E., Kahl, W.-A., Jöns, N., Moskowit, B., & Berquo, T. S. (2014). Magnetite in seafloor serpentinite—Some like it hot. *Geology*, 42, 135–138. <https://doi.org/10.1130/G35068.1>
- Kyser, T. K., O'Hanley, D. S., & Wicks, F. J. (1999). The origin of fluids associated with serpentinization processes: Evidence from stable-isotope compositions. *The Canadian Mineralogist*, 37, 223–237.
- Lagabriele, Y., & Lemoine, M. (1997). Alpine, Corsican and Apennine ophiolites: The slow-spreading ridge model. *Comptes Rendus de l'Académie des Sciences—Series IIA:—Earth and Planetary Science*, 325, 909–920. [https://doi.org/10.1016/s1251-8050\(97\)82369-5](https://doi.org/10.1016/s1251-8050(97)82369-5)
- Leake, B. E., Woolley, A. R., Arps, C. E. S., Rich, W. D., Gilbert, M. C., Grice, J. D., et al. (1997). Nomenclature of amphiboles: Report of the subcommittee on amphiboles of the international mineralogical association, commission on new minerals and mineral names. *The Canadian Mineralogist*, 35, 219–246.
- Le Breton, E., Brune, S., Ustaszewski, K., Zahirovic, S., Seton, M., & Müller, R. D. (2021). Kinematics and extent of the Piemont-Liguria Basin—implications for subduction processes in the Alps. *Solid Earth Discuss.*[preprint] accepted, 2021. accepted. <https://doi.org/10.5194/se-2020-161>
- Li, J.-L., Schwarzenbach, E. M., John, T., Ague, J. J., Huang, F., Gao, J., et al. (2020). Uncovering and quantifying the subduction zone sulfur cycle from the slab perspective. *Nature Communications*, 11, 514. <https://doi.org/10.1038/s41467-019-14110-4>
- Ludwig, K. A., Kelley, D. S., Butterfield, D. A., Nelson, B. K., & Früh-Green, G. (2006). Formation and evolution of carbonate chimneys at the Lost City hydrothermal field. *Geochimica et Cosmochimica Acta*, 70, 3625–3645. <https://doi.org/10.1016/j.gca.2006.04.016>
- Malvoisin, B. (2015). Mass transfer in the oceanic lithosphere: Serpentinization is not isochemical. *Earth and Planetary Science Letters*, 430, 75–85. <https://doi.org/10.1016/j.epsl.2015.07.043>
- Manatschal, G., & Müntener, O. (2009). A type sequence across an ancient magma-poor ocean-continent transition: The example of the western Alpine Tethys ophiolites. *Tectonophysics*, 473, 4–19. <https://doi.org/10.1016/j.tecto.2008.07.021>
- Marques, A. F. A., Barriga, F. J. A. S., & Scott, S. D. (2007). Sulfide mineralization in an ultramafic-rock hosted seafloor hydrothermal system: From serpentinization to the formation of Cu-Zn-(Co)-rich massive sulfides. *Marine Geology*, 245, 20–39. <https://doi.org/10.1016/j.margeo.2007.05.007>
- Marroni, M., Molli, G., Montanini, A., & Tribuzio, R. (1998). The association of continental crust rocks with ophiolites in the Northern Apennines (Italy): Implications for the continent-ocean transition in the Western Tethys. *Tectonophysics*, 292, 43–66. [https://doi.org/10.1016/s0040-1951\(98\)00060-2](https://doi.org/10.1016/s0040-1951(98)00060-2)
- Mayhew, L. E., & Ellison, E. T. (2020). A synthesis and meta-analysis of the Fe chemistry of serpentinites and serpentine minerals. *Philosophical Transactions of the Royal Society A: Mathematical, Physical and Engineering Sciences*, 378.20180420. <https://doi.org/10.1098/rsta.2018.0420>
- McCarthy, A., Chelle-Michou, C., Müntener, O., Arculus, R., & Blundy, J. (2018). Subduction initiation without magmatism: The case of the missing Alpine magmatic arc. *Geology*, 46, 1059–1062. <https://doi.org/10.1130/g45366.1>
- McDonough, W. F., & Sun, S.-S. (1995). The composition of the Earth. *Chemical Geology*, 120, 223–253. [https://doi.org/10.1016/0009-2541\(94\)00140-4](https://doi.org/10.1016/0009-2541(94)00140-4)
- Mével, C. (2003). Serpentinization of abyssal peridotites at mid-ocean ridges. *Comptes Rendus Geoscience*, 335, 825–852. <https://doi.org/10.1016/j.crte.2003.08.006>
- Miller, D. J., & Christensen, N. J. (1997). Seismic velocities of lower crustal and upper mantle rocks from the slow spreading Mid-Atlantic Ridge, south of the Kane transform fault. *Proceedings of the ocean drilling program, scientific results*, 153, 437–454.
- Molli, G. (1995). Pre-orogenic high temperature shear zones in an ophiolite complex (Bracco massif, Northern Apennines, Italy). In R. L. M. Vissers, & A. Nicolas (Eds.), *Mantle and lower crust exposed in oceanic ridges and in ophiolites*. Dordrecht: Kluwer Academic Publishers.
- Moody, J. B. (1976). Serpentinization: A review. *Lithos*, 9, 125–138. [https://doi.org/10.1016/0024-4937\(76\)90030-x](https://doi.org/10.1016/0024-4937(76)90030-x)
- Niu, Y. (2004). Bulk-rock major and trace element compositions of abyssal peridotites: Implications for mantle melting, melt extraction and post-melting processes beneath mid-ocean ridges. *Journal of Petrology*, 45, 2423–2458. <https://doi.org/10.1093/petrology/egh068>
- O'Hanley, D. S. (1996). *Serpentinites: Records of tectonic and petrological history*. New York, Oxford: Oxford university press.
- Paulick, H., Bach, W., Godard, M., De Hoog, J. C. M., Suhr, G., & Harvey, J. (2006). Geochemistry of abyssal peridotites (Mid-Atlantic Ridge, 15°20'N, ODP Leg 209): Implications for fluid/rock interaction in slow spreading environments. *Chemical Geology*, 234, 179–210. <https://doi.org/10.1016/j.chemgeo.2006.04.011>
- Peters, D., Bretscher, A., John, T., Scambelluri, M., & Pettke, T. (2017). Fluid-mobile elements in serpentinites: Constraints on serpentinization environments and element cycling in subduction zones. *Chemical Geology*, 466, 654–666. <https://doi.org/10.1016/j.chemgeo.2017.07.017>
- Piccardo, G. B., Padovano, M., & Guarnieri, L. (2014). The Ligurian Tethys: Mantle processes and geodynamics. *Earth-Science Reviews*, 138, 409–434. <https://doi.org/10.1016/j.earscirev.2014.07.002>
- Rampone, E., Hofmann, A. W., Piccardo, G. B., Vannucci, R., Bottazzi, P., & Ottolini, L. (1996). Trace element and isotope geochemistry of depleted peridotites from an N-MORB type ophiolite (Internal Liguride, N. Italy). *Contributions to Mineralogy and Petrology*, 123, 61–76. <https://doi.org/10.1007/s004100050143>
- Rehkämper, M., & Hofmann, A. W. (1997). Recycled ocean crust and sediment in Indian Ocean MORB. *Earth and Planetary Science Letters*, 147, 93–106.
- Rouméjon, S., Früh-Green, G. L., Orcutt, B. N., & Party, I. E. S. (2018). Alteration heterogeneities in peridotites exhumed on the southern wall of the Atlantis Massif (IODP Expedition 357). *Journal of Petrology*, 59, 1329–1358. <https://doi.org/10.1093/petrology/egy065>
- Sakai, R., Kusakabe, M., Noto, M., & Ishii, T. (1990). Origin of waters responsible for serpentinization of the Izu-Ogasawara-Mariana forearc seamounts in view of hydrogen and oxygen isotope ratios. *Earth and Planetary Science Letters*, 100, 291–303. [https://doi.org/10.1016/0012-821x\(90\)90192-z](https://doi.org/10.1016/0012-821x(90)90192-z)
- Salter, V. J. M., & Stracke, A. (2004). Composition of the depleted mantle. *Geochemistry, Geophysics, Geosystems*, 5, 1–27. <https://doi.org/10.1029/2003gc000597>
- Scambelluri, M., Müntener, O., Ottolini, L., Pettke, T. T., & Vannucci, R. (2004). The fate of B, Cl and Li in the subducted oceanic mantle and in the antigorite breakdown fluids. *Earth and Planetary Science Letters*, 222, 217–234. <https://doi.org/10.1016/j.epsl.2004.02.012>
- Schmidt, M. W. (1992). Amphibole composition in tonalite as a function of pressure: An experimental calibration of the Al-in-hornblende barometer. *Contributions to Mineralogy and Petrology*, 110, 304–310. <https://doi.org/10.1007/bf00310745>

- Schwarzenbach, E. M., Caddick, M. J., Beard, J. S., & Bodnar, R. J. (2016). Serpentinization, element transfer, and the progressive development of zoning in veins: Evidence from a partially serpentinized harzburgite. *Contributions to Mineralogy and Petrology*, 171, 1–22. <https://doi.org/10.1007/s00410-015-1219-3>
- Schwarzenbach, E. M., Früh-Green, G. L., Bernasconi, S. M., Alt, J. C., & Plas, A. (2013). Serpentinization and carbon sequestration: A study of two ancient peridotite-hosted hydrothermal systems. *Chemical Geology*, 351, 115–133. <https://doi.org/10.1016/j.chemgeo.2013.05.016>
- Schwarzenbach, E. M., Früh-Green, G. L., Bernasconi, S. M., Alt, J. C., Shanks, III, W. C., III, Gaggero, L., & Crispini, L. (2012). Sulfur geochemistry of peridotite-hosted hydrothermal systems: Comparing the Ligurian ophiolites with oceanic serpentinites. *Geochimica et Cosmochimica Acta*, 91, 283–305. <https://doi.org/10.1016/j.gca.2012.05.021>
- Schwarzenbach, E. M., Gill, B. C., & Johnston, D. T. (2018). Unraveling multiple phases of sulfur cycling during the alteration of ancient ultramafic oceanic lithosphere. *Geochimica et Cosmochimica Acta*, 223, 279–299. <https://doi.org/10.1016/j.gca.2017.12.006>
- Shanks, W. C., Böhlke, J. K., & Seal, R. R. (1995). *Stable isotopes in mid-ocean ridge hydrothermal systems Interactions between fluids minerals, and organisms*. Washington D.C. American Geophysical Union.
- Snow, J. E., & Dick, H. J. B. (1995). Pervasive magnesium loss by marine weathering of peridotite. *Geochimica et Cosmochimica Acta*, 59, 4219–4235. [https://doi.org/10.1016/0016-7037\(95\)00239-v](https://doi.org/10.1016/0016-7037(95)00239-v)
- Snow, J. E., Hart, S. R., & Dick, H. J. B. (1993). Orphan strontium-87 in Abyssal peridotites: Daddy was a granite. *Science*, 262, 1861–1863. <https://doi.org/10.1126/science.262.5141.1861>
- Strating, H. (1991). *The evolution of the Piemonte-Ligurian ocean: A structural study of ophiolite complexes in Liguria (NW Italy)*. Utrecht .
- Sun, S.-S., & McDonough, W. F. (1989). Chemical and isotopic systematics of oceanic basalts: Implications for mantle composition and processes. *Geological Society, London, Special Publications*, 42, 313–345. <https://doi.org/10.1144/gsl.sp.1989.042.01.19>
- Treves, B., Kickmott, D., & Vaggelli, G. (1995). Texture and microchemical data of oceanic hydrothermal calcite veins, Northern Apennine ophiolite. *Ophioliti*, 20, 111–122.
- Treves, B. E., & Harper, G. D. (1994). Exposure of serpentinites on the ocean floor: Sequence of faulting and hydrofracturing in the northern Apennine Ophiolite. *Ophioliti*, 19b.
- Tribuzio, R., Garzetti, F., Corfu, F., Tiepolo, M., & Renna, M. R. (2016). U-Pb zircon geochronology of the Ligurian ophiolites (Northern Apennine, Italy): Implications for continental breakup to slow seafloor spreading. *Tectonophysics*, 666, 220–243. <https://doi.org/10.1016/j.tecto.2015.10.024>
- Tribuzio, R., Renna, M. R., Dallai, L., & Zanetti, A. (2014). The magmatic-hydrothermal transition in the lower oceanic crust: Clues from the Ligurian ophiolites, Italy. *Geochimica et Cosmochimica Acta*, 130, 188–211. <https://doi.org/10.1016/j.gca.2014.01.010>
- Tribuzio, R., Thirlwall, M. F., & Vannucci, R. (2004). Origin of the Gabbro-Peridotite association from the Northern Apennine ophiolites (Italy). *Journal of Petrology*, 45, 1109–1124. <https://doi.org/10.1093/petrology/egh006>
- Tucholke, B. E., Behn, M. D., Buck, W. R., & Lin, J. (2008). Role of melt supply in oceanic detachment faulting and formation of megamullions. *Geology*, 36, 455–458. <https://doi.org/10.1130/g24639a.1>
- Ulmer, P., & Trommsdorff, V. (1995). Serpentine stability to mantle depths and subduction-related magmatism. *Science*, 268, 858–861. <https://doi.org/10.1126/science.268.5212.858>
- Veizer, J., Ala, D., Azmy, K., Bruckschen, P., Buhl, D., Bruhn, F., et al. (1999). $^{87}\text{Sr}/^{86}\text{Sr}$, $\delta^{13}\text{C}$ and $\delta^{18}\text{O}$ evolution of Phanerozoic seawater. *Chemical Geology*, 161, 59–88. [https://doi.org/10.1016/S0009-2541\(99\)00081-9](https://doi.org/10.1016/S0009-2541(99)00081-9)
- Vils, F., Tonarini, S., Kalt, A., & Seitz, H.-M. (2009). Boron, lithium and strontium isotopes as tracers of seawater-serpentinite interaction at Mid-Atlantic ridge, ODP Leg 209. *Earth and Planetary Science Letters*, 286, 414–425. <https://doi.org/10.1016/j.epsl.2009.07.005>
- Vogel, M. (2016). Peridotite-hosted hydrothermal systems past and present: Serpentinization, metasomatism and carbonate precipitation in modern and jurassic ultramafic seafloor, Dr. Sc., Department of Earth Sciences, ETH Zurich, Zurich, Switzerland, 142 pp.
- von Damm, K. L. (1990). Seafloor hydrothermal activity: Black smoker chemistry and chimneys. *Annual Review of Earth and Planetary Sciences*, 18(173). <https://doi.org/10.1146/annurev.earth.18.050190.001133>
- von Damm, K. L. (1995). Controls on the chemistry and temporal variability of seafloor hydrothermal fluids. In S. Humphris, R. A. Zierenberg, L. Mullineaux, & R. E. Thomson (Eds.), *Seafloor hydrothermal systems: Physical, chemical, biological, and geological interactions*. Wenner, D. B., & Taylor, H. P. (1973). Oxygen and hydrogen isotope studies of the serpentinization of ultramafic rocks in oceanic environments and continental ophiolite complexes. *American Journal of Science*, 273, 207–239. <https://doi.org/10.2475/ajs.273.3.207>
- Wenner, D. B., & Taylor, H. P. (1974). D/H and $\text{O}^{18}/\text{O}^{16}$ studies of serpentinization of ultramafic rocks. *Geochimica et Cosmochimica Acta*, 38, 1255–1286. [https://doi.org/10.1016/0016-7037\(74\)90120-3](https://doi.org/10.1016/0016-7037(74)90120-3)
- Whitmarsh, R. B., Manatschal, G., & Minshull, T. A. (2001). Evolution of magma-poor continental margins from rifting to seafloor spreading. *Nature*, 413, 105–154. <https://doi.org/10.1038/35093085>
- Wierzbowski, H., Anczkiewicz, R., Pawlak, J., Rogov, M. A., & Kuznetsov, A. B. (2017). Revised middle-upper Jurassic strontium isotope stratigraphy. *Chemical Geology*, 466, 239–255. <https://doi.org/10.1016/j.chemgeo.2017.06.015>
- Zaccarini, F., & Garuti, G. (2008). Mineralogy and chemical composition of VMS deposits of northern Apennine ophiolites, Italy: Evidence for the influence of country rock type on ore composition. *Mineralogy and Petrology*, 94, 61–83. <https://doi.org/10.1007/s00710-008-0010-9>